Final Report

Development of Calcined Clays as Pozzolanic Additions in Portland Cement Concrete Mixtures

FDOT Contract Number: BDV25-977-38

Date: August 2018

Submitted to

Research Center (Research.center@dot.state.fl.us)

The Florida Department of Transportation

Research Center

605 Suwannee Street, MS 30

Tallahassee, FL 32399

c/o Dr. Harvey DeFord

Structural Materials Research Specialist

State Materials Office

5007 NE 39th Avenue

Gainesville, FL 32609

Phone: (352)955-6671

Email: Harvey.deford@dot.state.fl.us

Submitted by

Principal Investigator: Dr. A. Zayed

Department of Civil and Environmental Engineering

University of South Florida

4202 E Fowler Avenue; ENB 118

Tampa, FL 33620-5350

Email: zayed@usf.edu

Service Date: January 2017 – August 2018

Disclaimer

The opinions, findings, and conclusions expressed in this publication are those of the authors and not necessarily those of the State of Florida Department of Transportation (FDOT) or the U.S. Department of Transportation (USDOT) or the Federal Highway Administration (FHWA).

Approximate Conversions to SI Units (from FHWA)

Symbol	When You Know	Multiply By	To Find	Symbol
Length				
in	inches	25.4	millimeters	mm
ft	feet	0.305	meters	m
yd	yards	0.914	meters	m
mi	miles	1.61	kilometers	km
Area				
in^2	square inches	645.2	square millimeters	mm^2
ft^2	square feet	0.093	square meters	m^2
yd^2	square yard	0.836	square meters	m^2
mi^2	square miles	2.59	square kilometers	km^2
Volume				
fl oz	fluid ounces	29.57	milliliters	mL
gal	gallons	3.785	liters	L
ft^3	cubic feet	0.028	cubic meters	m^3
yd^3	cubic yards	0.765	cubic meters	m^3
NOTE: volumes greater than 1000 L shall be shown in m^3				
Mass				
oz	ounces	28.35	grams	g
lb	pounds	0.454	kilograms	kg
Temperature (exact degrees)				
°F	Fahrenheit	5 (F-32)/9 or (F-32)/1.8	Celsius	°C
Illumination				
fc	foot-candles	10.76	lux	lx
fl	foot-Lamberts	3.426	candela/m^2	cd/m^2
Force and Pressure or Stress				
lbf	pound-force	4.45	newtons	N
lbf/in^2	pound-force per square inch	6.89	kilopascals	kPa

Technical Report Documentation Page

1. Report No.	2. Government Accession No.	3. Recipient's Catalog No.
4. Title and Subtitle Development of Calcined Clays as Pozzolanic Additions in Portland Cement Concrete Mixtures		5. Report Date August 2018 6. Performing Organization Code
7. Author(s) A. Zayed, N. Shanahan, A. Sedaghat, Y. Stetsko, and B. Lorentz		8. Performing Organization Report No.
9. Performing Organization Name and Address Department of Civil and Environmental Engineering University of South Florida 4202 E Fowler Avenue; ENB 118 Tampa, FL 33620-5350		10. Work Unit No. 11. Contract or Grant No. BDV25-977-38
12. Sponsoring Agency Name and Address U.S. Department of Transportation-Florida Department of Transportation		13. Type of Report and Period Covered Final Report; 1/18/2017-08/31/2018 14. Sponsoring Agency Code
15. Supplementary Notes None		

16. Abstract

A number of clay sources in the state of Florida were characterized in this study. It was determined that field material contains a substantial portion of sand, approximately 65-80%, which needs to be beneficially processed before the material can be used as a pozzolan. The clay fraction met the chemical oxide composition requirements of ASTM C618. All samples had a sum of SiO_2, Al_2O_3, and Fe_2O_3 oxides above 70%, and their SO_3 content was below 4%. Additionally, the clay fraction had a high kaolinite content, 70-90%, which indicates a good potential of producing a high-quality pozzolanic material on calcination. It was determined that complete dehydroxylation of all the clay samples occurred at 600˚C and that further heating to 800˚C did not increase the amorphous content of the calcined clays. Pozzolanic activity of the material calcined at 600˚C was evaluated by compressive strength testing at 7 and 28 days at a replacement level of 10%. The results showed that the Florida clays obtained can be calcined for use in portland cement concrete materials, and are capable of yielding strength indices meeting the requirements of ASTM C618 at a 10% replacement level, and are, therefore, suitable for use in concrete as Class N natural pozzolans.

17. Keywords.	18. Distribution Statement
Portland cement, calcined clay, kaolinite, X-ray fluorescence, X-ray diffraction, thermogravimetric analysis, mortar compressive strength.	No restrictions.

19. Security Classification (this report)	20. Security Classification (this page)	21. Pages	22. Price
Unclassified	Unclassified	91	

Form DOT F 1700.7 (8-72) Reproduction of completed page authorized

Acknowledgement

This work has been sponsored by the Florida Department of Transportation (FDOT) and the Federal Highway Administration (FHWA). The Principal Investigator appreciates the valuable discussions with Dr. Harvey DeFord, Project Manager, and Mr. Michael Bergin, PE. The authors would like to thank Mr. David Hudson with the FDOT State Materials Office (SMO) for his assistance with this research.

EXECUTIVE SUMMARY

1.1 Background

Supplementary cementitious materials (SCMs) are widely used in structural concrete in order to achieve improved durability. Currently, the most commonly used SCM in Florida is Class F fly ash, as it has a proven record of performance; however, the supply of Class F fly ash is expected to diminish in the near future, and there is a need to identify a material that can be used in its place. Metakaolin (MK), which is a fairly new SCM, can potentially fill this role, although its cost is significantly higher than that of fly ash. MKs that are currently on the market are produced from high purity kaolinite clay, which increases the cost of MK.

Recently, a few studies have explored the possibility of using low-grade kaolin clay as well as other clays, such as bentonite, illite, and montmorillonite, for producing a pozzolanic material for use in concrete production. The amorphous content, chemical and mineralogical composition of the starting clay, and calcining temperature have been shown to affect the quality of the resulting pozzolanic material. The main goal of this study is to evaluate if Florida clays can be developed into pozzolanic materials that can be used to replace fly ash in Florida Department of Transportation (FDOT) concrete mixtures.

1.2 Research Objectives

The objectives of the proposed research are (1) evaluate the quality of various clay sources available in Florida in terms of their chemical and mineralogical composition and amorphous content through the use of x-ray fluorescence and x-ray diffraction techniques, (2) explore different calcination temperatures and accompanying phase transformation for various clay samples through the use of x-ray diffraction (XRD) or other techniques, and (3) evaluate the reactivity of calcined pozzolanic materials in combination with ordinary portland cement (OPC) through the use of mortar compressive strength. Satisfying the objectives of this study will provide the Florida Department of Transportation with the scientific knowledge on the locally available clay-based materials and their potential use in structural concrete.

1.3 Main Findings

The main findings of this study are as follows:

- A number of potential clay sources were identified in the state of Florida. The obtained field samples contained approximately 65% to 80% sand (material retained on the 45-μm sieve). The fraction passing the 45-μm sieve met the chemical oxide composition requirements of ASTM C618: minimum of 70.0% for SiO_2+Al_2O_3+Fe_2O_3 and SO_3 content of less than 4%. The kaolin content of the #325 mesh material was determined by XRD and thermogravimetric analyses (TGA) and ranged from approximately 70% to 90%, indicating a good potential of producing a high-quality pozzolanic material on calcination.
- A detailed step-wise temperature study performed for one clay showed that complete dehydroxylation occurs at 600˚C. All the clays were calcined at 600˚C and 800˚C, and their amorphous content was quantified using Rietveld refinement. No change in amorphous content was detected on heating above 600˚C, confirming that all the clays were completely dehydroxylated at this temperature.
- Pozzolanic activity of the material calcined at 600˚C was evaluated by compressive strength testing at 7 and 28 days. The results showed that the Florida kaolinitic clays obtained are capable of being calcined to produce a pozzolanic material that can be used to replace portland cement in concrete and yield strength indices that meet the requirements of ASTM C618 at a 10% replacement level, and are, therefore, suitable for use in concrete as Class N natural pozzolans.

1.4 Recommendations

Based on the findings of this study, it is recommended that the Florida Department of Transportation proceed to Phase II of this project in order to further evaluate the effect of calcined clays on the properties of cementitious mixtures, including strength and durability.

1.5 Recommendations for Future Study

Calcined clays need to be further evaluated in terms of their effect on concrete long-term durability prior to implementation and use as a supplementary cementitious material.

TABLE OF CONTENTS

LIST OF FIGURES

LIST OF TABLES

Chapter 1. Literature Review

1.1. Introduction

Class F fly ash has been historically used in Florida to improve fresh and hardened concrete properties and to reduce cost. However, recent concerns over fly ash availability necessitate exploration of other materials that could be used in its place [1]. One of the possibilities is the use of clay, which can be calcined to produce a pozzolanic material ([1], [2]). The possibility of using lower-grade mineral clays is particularly attractive since there are large clay deposits worldwide [2].

There is some confusion in the cement and concrete literature regarding the distinction between clays and clay minerals. This is not surprising, as there is currently "no uniform nomenclature for clay" or clay minerals as pointed out by Bergaya and Lagaly [3]. The industrial classification of clays provided by [3] separates the clays into four different types based on their predominant minerals: kaolins, bentonites, palygorskite (attapulgite), and sepiolite, and 'common clays.' Kaolins are primarily composed of kaolinite. The major minerals in bentonites are Ca- or Na-montmorillonite. Palygorskite and sepiolite are named after their respective primary mineral; while 'common clays' are typically composed of illite and smectite. Clays that are typically calcined and used in concrete as supplementary cementitious materials (SCM) belong to the kaolin group.

Clays belong to a family of minerals called phyllosilicates, which are made up of tetrahedral silicate sheets and octahedral metal oxide (or hydroxide) sheets [4]. All 1:1 clay minerals have tetrahedral silicate sheets and octahedral metal oxide sheets that are alternately stacked on top of each other. In 2:1 clay minerals, there are two silicate sheets on each face of the octahedral sheet.

Kaolinite, halloysite, dickite, nacrite, and livesite are clays belonging to the kaolin group, which are 1:1 clays made up of Si-O tetrahedral and Al-O(OH) octahedral sheets. Together they form a "composite kaolin layer" with distorted Si-O and Al-O distances [5]. Bentonites, palygorskite, and sepiolite are 2:1 clays.

An important parameter in the clay structure that influences calcined clay reactivity is the degree of order/disorder of the clay minerals. It can be determined by calculating P_0, which is a ratio of the intensities of the 3620 cm^{-1} and 3700 cm^{-1} FTIR bands. The 3620 cm^{-1} band corresponds to the "inner OH groups attached to aluminum and oxygen atoms" within the octahedral layer, while the 3700 cm^{-1} band is associated with the "inner surface OH groups," which are also attached to the surface of the octahedral layer and are able to bond with the tetrahedral silica layer through hydrogen bonding. These hydrogen bonds are stretched with "ab displacements or isomorphous substitutions" causing an increase in the degree of disorder of the clay [6]. Bich [6] reported that clays with $P_0 > 1$ are well-ordered, while clays with $P_0 < 1$ are disordered.

Calcined clays fall under the Class N classification of ASTM C618. For this classification, the standard outlines the following requirements in terms of chemical composition: a minimum of 70.0% for $SiO_2+Al_2O_3+Fe_2O_3$, and a maximum of 4.0% for SO_3. Based on the compositions of various clay minerals reported in the literature ([7]–[15]), the majority of calcined clays should be able to satisfy both of these requirements. In practice, compliance may depend on the amount of associated minerals in the clay ([3], [16]). Typically, clays are found together with quartz, carbonates, feldspars, and oxides and hydroxides of aluminum and iron, which should not affect either of the Class N requirements. Possible non-compliance can result from the presence of sulfate-rich associated minerals, such as alunite ($KAl_3(SO_4)_2(OH)_6$), the presence of which was reported by ([8], [17], [18]) in kaolin samples. Kakali et al. [17] reported that although alunite decomposes at 500-900˚C, "there was detectable sulfate content" after heating to 950˚C. However, the exact amount of sulfate after calcination was not reported in this study. Although associated minerals are typically considered non-reactive, Ghorbel and Samet [19] suggested that the presence of Fe-bearing goethite and hematite may increase reactivity of calcined kaolinite up to an Fe_2O_3 content of 2.7%, above which the authors observed a decrease in reactivity as measured by compressive strength at 7-90 days.

In terms of physical properties, ASTM C618 specifies a maximum percent retained on a 45-μm sieve of 34%, a maximum autoclave expansion of 0.8%, a minimum strength activity index of 75%, a maximum water requirement of 115%, and a uniformity specified by a maximum

variation in the measured density of 5%. The current literature does not typically address these requirements, with the exception of the strength index.

1.2. Transformation of Clay Minerals on Heating

Thermal behavior of clays can be divided into 3 general stages: dehydration, dehydroxylation, and recrystallization ([17], [20]). Kakali et al. [17] specify the end of the dehydration stage occurs at 100˚C, while Mohammed [20] states that it can extend up to 200˚C. The temperature ranges for the dehydroxylation and recrystallization stages vary depending on the clay mineralogy. During the dehydration stage, as free water is evaporated, no changes occur to the clay structure. Mass loss during dehydration and dehydroxylation periods can be measured using thermogravimetric analysis (TGA).

In the dehydroxylation stage, hydroxyl groups are removed from the clay structure resulting in a collapse of the basal spacing and loss of crystallinity ([17], [20]–[23]). The degree of dehydroxylation (D_{TG}) can be calculated from TGA measurements using the formula proposed by Rahier et al. [24]:

$$D_{TG} = 1\text{-}m/m_0 \qquad \text{Equation 1}$$

where m and m_0 are residual and maximum mass loss, respectively. Rahier et al. [24] dried the samples at 250˚C prior to TGA analysis, so the water of dehydration was not considered to be part of m and m_0.

In the case of kaolinite, the following transformation occurs during the dehydroxylation stage [25]:

$$Al_2O_3{\cdot}2SiO_2{\cdot}2H_2O \text{ (kaolinite)} \xrightarrow{450-700^\circ C} Al_2O_3{\cdot}2SiO_2 \text{ (metakaolinite)} + 2H_2O \text{ (g)}$$

The calcined material obtained during the dehydroxylation stage is pozzolanic and can potentially be used in concrete. Among the clay minerals, calcined kaolinite has been reported to be the most reactive, followed by montmorillonite, with other clay minerals showing lower reactivity [16]. The high reactivity of kaolinite is most likely due to the higher amount of hydroxyl groups present in its structure compared to the other clay minerals [7]. In addition to higher

reactivity, the dehydroxylation (calcination) temperature of pure kaolinite is also lower than that of other clay minerals ([20], [26]).

Further increase in the temperature, above the dehydroxylation temperature, leads to formation of crystalline phases (recrystallization stage), which decreases the reactivity of calcined clay. When metakaolinite is heated above 925˚C, spinel forms, which is transformed into mullite above 1050˚C. Above 1200˚C amorphous silica is converted into cristobalite, and the calcined clay becomes completely crystalline [25]:

$2(Al_2O_3 \cdot 2SiO_2)$ (metakaolinite) $\xrightarrow{925-1050^\circ C}$ $2Al_2O_3 \cdot 3SiO_2$ (spinel) + SiO_2 (amorphous silica)

$3(2Al_2O_3 \cdot 3SiO_2)$ (spinel) $\xrightarrow{\geq 1050^\circ C}$ $2(3Al_2O_3 \cdot 2SiO_2)$ (mullite) + $5SiO_2$ (amorphous silica)

SiO_2 (amorphous silica) $\xrightarrow{\geq 1200^\circ C}$ SiO_2 (cristobalite)

Phase transformation of different clay minerals on heating can be followed by differential thermal analysis (DTA), where temperature changes of a sample of calcined material upon heating is measured against an inert sample at the same temperatures. Endothermic or exothermic peaks are generated during phase transformations, crystallization, and melting, which occur during specific temperature ranges for each mineral [27]. Both DTA and TGA can be used to determine the temperature ranges of dehydration, dehydroxylation and recrystallization of clays.

1.3. Reactivity of Calcined Clays

The use of metakaolin (MK) obtained from the calcination of high-purity kaolins has been shown to be very effective in improving concrete strength and durability ([10], [28]–[35]). However, since deposits of pure kaolin are rare, the cost of metakaolin is high due to additional separation and processing requirements. Recently, there has been a lot of interest in using calcined, naturally-occurring clays as supplementary cementitious materials (SCMs) that could potentially provide improved concrete properties, but at a lower cost. These natural clays have a significantly lower kaolinite content (lower-grade) compared to the high-grade kaolins used for MK production, or do not contain any kaolinite, with their pozzolanic properties coming from calcination of other

clay minerals. Since kaolinite has the highest reactivity and the lowest calcination temperature compared to other clay minerals ([16], [20], [26]), the majority of research has been focused on natural clays containing kaolinite.

Typical clay deposits, including those containing kaolinite, contain differing proportions of several clay minerals. Since dehydroxylation temperatures for pure clay minerals range from 600-650˚C for kaolinite ([7], [36], [37]) to 950˚C for smectite [20], optimum calcination temperature will be determined by the specific clay mineralogy. Optimum calcination temperature is generally defined as the temperature resulting in the maximum reactivity of the calcined material. A large number of methods are currently used to assess actual or potential reactivity of calcined clay, including the Chapelle and Frattini tests, x-ray diffraction (XRD) to determine the amount of amorphous material after calcination, TGA to determine the degree of dehydroxylation, and compressive strength. For the Chapelle test, 1 g of calcined clay is mixed with 1 g of CH in water at 100˚C and boiled for 16 hours, after which the remaining free CH is quantified by "sucrose extraction and titration with a HCl solution" [17]. In the Frattini test, 30% of the pozzolanic material is mixed with 70% of cement in water. After curing for 7-28 days at 40˚C, the solution is analyzed for calcium and hydroxide ions to determine the ability of the pozzolan to remove calcium ions from solution [38]. These tests do not always result in the same optimum calcination temperatures as XRD; the Chapelle and Frattini tests reflect only the chemical effect of the calcined material on cement hydration, while compressive strength originates from both chemical and physical effects.

Bich et al. [6] investigated the effect of the degree of dehydroxylation on reactivity of high-content kaolinite clays. Three clays with kaolinite contents of 75 - 87.3% were calcined at 650˚C for variable amounts of time to vary the degree of dehydroxylation, which was calculated from DTA measurements. Degree of dehydroxylation varied from 50 to 100%. The authors noted that for a clay with a disordered structure, the time required to achieve complete dehydroxylation was significantly shorter compared to the clays with a high degree of order (45 min vs. 5 h), so the removal of hydroxyl ions is significantly easier in a disordered structure. Reactivity of the calcined clays was measured in terms of lime consumption in pastes prepared with 50% CH and 50% calcined material at normal consistency. The authors concluded that there was no relationship between lime consumption and degree of dehydroxylation at 7 days, although a better correlation

between these parameters was observed at 28 days. However, even at 28 days there was a lot of scatter in the data suggesting that other parameters, besides the degree of dehydroxylation, may be affecting calcined clay reactivity.

Tironi et al. [38] investigated five kaolinitic clays with a range of kaolinite contents from high (76 and 94%) to low (16%). Fourier transform infrared (FTIR) spectra were used to determine whether the structures of raw clays were ordered or disordered. The highest- and the lowest-kaolinite-content clays had an ordered structure, while the rest of the clays had a disordered structure. Clays were calcined at 700˚C and ground "until 100% of mass passed through the 45-μm sieve (# 325)" [38]. The resulting surface area was measured using the Blaine air permeability test, which showed large differences in the fineness of the calcined clays (981 to 2287 m^2/kg). Not surprisingly, two clays with highest Blaine fineness values (2287 and 1865 m^2/kg) were reported as most reactive as determined by the Frattini test, electrical conductivity measurements, and compressive strength measurements at 7-90 days. Since the highest kaolinite-content clay had an ordered structure in addition to lower fineness (1461 m^2/kg), and all the results follow the trend of the fineness, the authors used ANOVA to determine if the effects of fineness, degree of order/disorder, and kaolinite content of the uncalcined clays on compressive strength was significant. All the parameters were concluded to be significant, and their significance varied with age. Significance of kaolinite content of clay increased with age as well as the degree of order/disorder, while significance of clay fineness decreased with age.

Krishnan & Bishnoi [39] evaluated the reactivity of 2 natural clays with low and high kaolinite contents of 20 and 80%, respectively. Both clays were calcined at 800˚C followed by 8 hours of soaking. After that, the calcined clays were interground with clinker, 2 different limestones (high- and low-quality), and gypsum. Unfortunately, the calcium carbonate content of the two limestones was not specified. The clay content was fixed at 30%, limestone content was 15%, gypsum was added at 5%, and the remaining 50% of the mixture was clinker. The authors reported poor lime reactivity of the 20% kaolinite clay. Compressive strength of mortar cubes, prepared with the calcined clays at a w/cm ratio of 0.45, was also measured and compared to the performance of OPC and OPC+30% fly ash. Compressive strengths of mortar cubes prepared with 20% kaolinite clay and high-quality limestone were slightly higher than those of OPC at 7-90 days. Compressive strengths of 20% kaolinite clay and low-quality limestone were similar to those of

the mortar cubes containing fly ash. A significant increase in compressive strength was achieved with 80% kaolinite clay regardless of the limestone quality. Similar results were obtained for concrete, where mixes containing 20% kaolinite clay showed similar performance to the mix containing fly ash, while 80% kaolinite clay strengths were similar to that of OPC.

Pierkes et al. [40] compared the performance of three clays, identified as illitic, kaolinitic, and chloritic, with 4 different OPCs. Clays were calcined at temperatures ranging from 800 to 1200˚C, and compressive strengths were compared for 20% cement replacement levels. The authors concluded that there is little contribution to compressive strength development from the calcined clays before 7 days, and the effect of calcined clay could only be observed after this age. As expected, different optimal calcination temperatures were obtained for each clay, based on compressive strength measurements. Additionally, for the illitic and kaolinitic clays, which had similar mineralogical compositions (illite/muscovite, kaolinite, quartz, and feldspar) and differed mainly in their kaolinite content, the optimum calcination temperature decreased with increasing kaolinite content. It appears that the optimum calcination temperature depends not only on the clay minerals present, but also on their relative amounts. Since it may not be possible to accurately quantify all the clay minerals present in a sample because crystal structures for a number of clay minerals have not been investigated, it may be difficult to predict the optimum calcination temperature based on mineralogy alone. Additionally, other parameters, such as particle size [10] or fineness [38] and degree of order/disorder [38], have an effect on optimum calcination temperature.

Kakali et al. [17] compared the reactivity of 5 different clays with a range of kaolinite contents (38-96%), as well as variable kaolinite crystallinity (degree of order/disorder). Clays were calcined at 650˚C and their reactivities were evaluated using the Chapelle test. The results were expressed both in terms of CH consumption per gram of calcined clay, as well as per gram of metakaolinite in the calcined samples. The authors observed that when the results were normalized by the total mass of calcined clay, the samples containing more metakaolin appear to be more reactive; however, when the results are normalized by the amount of metakaolin, reactivity was higher for the clays with a greater degree of disorder. Similar to Tironi et al. [38], Kakali et al. [17] concluded that the degree of order/disorder of the raw clay has an effect on the reactivity of the calcined pozzolan, with less crystalline clays resulting in more reactive pozzolans. Influence

of these clays on compressive strength at 10 and 20% cement replacement was reported by Badogiannis et al. [8]. The onset of pozzolanic reaction for all clays was observed at 7 days, which is consistent with observations by Pierkes et al. [40]. While compressive strengths of low-kaolinite clays (38 and 39% kaolinite) were lower than those of high-kaolinite clays (> 52% kaolinite), they were equal to or greater than the strength of OPC after 7 days.

Alujas et al. [41] looked at the effect of calcination temperature on a clay containing 40% kaolinite and 40% of a mixture of illite and montmorillonite. While a range of calcination temperatures was investigated in this study, 800˚C was determined to be optimal based on both the highest compressive strengths attained at 7 and 90 days, and the highest heat evolution measured by isothermal calorimetry.

On the contrary, Rasmussen et al. [42] reported the optimum calcination temperature for a kaolinite clay sample to be 900˚C, while for an illite/smectite sample it was around 800˚C for the soak-calcination method. The kaolinite clay used by Rasmussen et al. contained 5-10% quartz; unfortunately, its kaolinite content was not reported. The illite/smectite clay contained 10% quartz and 10% calcite. The authors reported that evidence of the clay reaction could be seen after 3 days. At 28 days, compressive strengths of kaolin clay mortars were higher than that of the OPC mortar. As for calcined illite/smectite clay, its compressive strength was reported to be 96% of the strength of OPC at 28 days.

Beuntner and Thienel [43] investigated the pozzolanic activity of a clay containing 25% kaolinite, 30% mica, 11% illite, and 6% chlorite. Optimum calcination temperature was determined to be in the range of 700 - 800˚C, which is in line with the results reported by [41]. Beuntner and Thienel [43] determined the optimum temperature based on solubility of calcined samples in an alkaline solution, which is a rapid test of pozzolanic activity. For the clay calcined at the optimum temperature, compressive strength of mortar at 28 days with 20% cement replacement was reported to be greater than that of OPC.

Taylor-Lange et al. [36] studied the reactivity of calcined kaolin-bentonite clays. A natural clay consisting of a mixture of Ca-bentonite and kaolin with approximately 25% kaolinite, as determined by semi-quantitative XRD analysis, and a laboratory-prepared blend of kaolin and Na-bentonite (approximately 40% kaolinite) were evaluated. Pure kaolin was also used in this study

as a reference. The calcination temperature for all materials was varied from 600 to 950˚C. Optimum calcination temperatures were then determined based on the amount of amorphous material after calcination as determined by XRD, and were 650˚C for pure kaolin, 930˚C for Ca-bentonite/kaolinite, and 830˚C for Na-bentonite/kaolinite blends. These materials were then used to prepare mortar cubes at a 15% cement replacement level for compressive strength testing. As expected, calcined kaolin showed the highest strength development. The Ca-bentonite blend showed similar compressive strengths to those of pure OPC at all ages, except at 90 days when its strength was higher. The Na-bentonite blend had lower strengths during the first 3 days, after which its strength was higher than that of OPC and the Ca-bentonite blend. It should be noted that the strengths of Na- and Ca-bentonite were very similar at 90 days. However, the authors concluded that Na-bentonite blend "proved to be the most reactive" compared to the Ca-bentonite blend. They further suggested that "sodium bentonite blended with 35 wt.% kaolinite has the potential to be used as a moderately reactive SCM in industry." Since neither of the bentonite clays was examined on its own, and the blended clays had variable amounts kaolinite, it is not clear if the Na-bentonite blended with kaolin would actually be more reactive than Ca-bentonite blended with an equal amount of kaolin. The lower calcination temperature and slightly higher compressive strengths of the Na-bentonite blend could be attributed to its higher kaolinite content.

Prior to this study, He et al. [13] compared the reactivity of calcined Na- and Ca-montmorillonite, which are the main components of Na- and Ca-bentonite, respectively. The samples were calcined at 730, 830, and 930˚C, and their effects on compressive strength were evaluated by preparing mortar cubes at a 30% cement replacement level. It should be noted that the w/cm ratio was varied from 0.6 to 0.8 to maintain constant flow, and compressive strength results were normalized using Feret's formula. Based on compressive strength measurements, both Na- and Ca-montmorillonite had the same optimum calcination temperature of 830˚C. Additionally, compressive strengths of Ca-montmorillonite were notably higher than those of Na-montmorillonite at all ages after 7 days, which is contrary to the results reported by Taylor-Lange et al. [36]. While reactivity of calcined bentonite may be different from that of calcined, pure montmorillonite, the results reported in [13] may have been affected by the variation in the w/cm ratio.

Garg and Skibsted [44] also investigated the use of pure montmorillonite as an SCM. It was observed that a calcination temperature of 800˚C resulted in maximum reactivity of calcined montmorillonite, which is consistent with the results of [13]. Although the reactivity of calcined montmorillonite, in combination with white portland cement, was found to be lower than that of metakaolin, the authors reported that it was similar to that of slag or fly ash.

He et al. [12] evaluated the effect of calcination temperature on pure clay minerals: kaolinite, illite, Ca-montmorillonite, Na-montmorillonite, mixed layer mica/smectite and sepiolite. Calcination temperature in this study was varied from 550 to 900˚C. The amorphous content of calcined clays was measured using x-ray diffraction (XRD). The greatest amorphous content for kaolin and Na-montmorillonite was observed at approximately 800˚C, after which it decreased due to formation of mullite in kaolinite and γ-Al_2O_3 in Na-montmorillonite. No drop in amorphous content with increase in calcination temperature was observed for the rest of the clay minerals. Calcination temperatures were also evaluated by differential thermal analysis (DTA), where the end of dehydroxylation for kaolinite was determined to be 650˚C; for Ca- and Na-montmorillonite, it was at 730 and 740˚C, respectively; 560˚C for mica/smectite, and 830˚C for sepiolite, which was contradictory to the XRD results, where the greatest amorphous content for kaolin and Na-montmorillonite was observed at 800˚C. Compressive strengths were also assessed for each mineral calcined at different temperatures. It is interesting to note that calcination temperatures required to achieve the highest compressive strength did not consistently correspond to the optimum calcination temperatures determined by XRD or DTA. For kaolinite and sepiolite, the optimum strength-based calcination temperatures were the same as those determined by DTA, while for Na-montmorillonite and mica/smectite, they corresponded to the optimum temperatures determined by XRD. For Ca-montmorillonite, no difference in amorphous content was observed in the 700 - 900˚C range by XRD, while optimum calcination temperature using compressive strength was determined to be 830˚C. This could be due to the difference in the fineness of the calcined clays, which is known to affect strength. A general correlation between strength and amount greater than 45 μm was reported in this study, although the R^2 value was rather low (0.66). This indicates a complex interaction between fineness and structural parameters of the clay minerals.

At optimum strength-based calcination temperatures, the highest compressive strengths were observed for kaolinite and Ca-montmorillonite. Although the strength of Na-montmorillonite was lower, it still exceeded the compressive strength of pure OPC. The authors concluded that illite and sepiolite were poor pozzolans, even though their compressive strengths were comparable to that of fly ash.

In a separate study [11], performance of illite was again classified as poor by He et al. In this work, three calcination temperatures (650˚C, 790˚C, and 930˚C) were selected to correspond to the beginning, middle, and end of the calcination range as determined by DTA. No significant improvement in compressive strength was observed with addition of illite calcined at 650˚C compared to uncalcined illite at all ages up to 91 days. Improvement in compressive strength with addition of material calcined at 790˚C and 930˚C could only be observed after 28 days, indicating a later-age reactivity of calcined illite. The highest compressive strengths were observed for 930˚C illite, which corresponded to approximately 80% and 90% of OPC strength at 28 and 91 days, respectively.

A similar study was conducted for sepiolite [14], where the sepiolite was heated to 370˚C, 570˚C, and 830˚C. The maximum compressive strengths were observed for the mortar incorporating material calcined at 830˚C. Unlike illite, calcined sepiolite contributes to strength gain between 7 and 28 days. Again, He et al. [14] concluded that sepiolite is a poor pozzolan, since compressive strengths after 7 days were approximately 84% of the OPC strengths.

Hollanders et al. [45] attempted to "understand the origin of the pozzolanic reactivity" of calcined clays. The authors selected eight different clays for their study: three kaolinites with different degrees of order/disorder; a halloysite, which has a similar structure to that of kaolinite; an illite; and three smectites (Na-montmorillonite, Ca-montmorillonite, and hectorite). Clays were calcined at maximum temperatures ranging from 500 to 900˚C. The authors identified 700˚C as the optimum calcination temperature for kaolinitic clays, including halloysite, based on the absence of kaolinite peaks as measured by XRD. However, for the kaolin sample with low degree of order/disorder, no kaolinite peaks were observed even at 500˚C, and only a small amount of crystalline kaolinite was detected for the kaolin sample with a medium degree of order/disorder. These results were confirmed by portlandite (CH) consumption at 28 days. For the highly-ordered

kaolin sample, CH consumption significantly increased for the sample calcined at 700˚C compared to the one calcined at 500˚C, while no change in portlandite consumption was observed on heating above 700˚C. For the samples with low and medium degrees of order/disorder, no significant changes in CH consumption were observed on heating above 500˚C. Loss of crystallinity for halloysite was also observed at 500˚C, which was consistent with CH consumption results. The authors concluded that for kaolinites, including halloysite, reactivity is dependent on the degree of order/disorder.

The researchers reported that a temperature of 900˚C was required for complete loss of crystallinity of Na-montmorillonite, although CH consumption at this temperature was lower than at 700 or 800˚C. Therefore, it appears that loss of crystallinity as measured by XRD may not always correlate to maximum reactivity, at least for Na-montmorillonite. For Ca-montmorillonite, complete calcination was achieved at 800˚C, which is in line with the CH consumption results. This is also consistent with the results of ([13], [44]). Additionally, CH consumption for Ca-montmorillonite calcined at 800˚C was notably higher than that of Na-montmorillonite, leading the authors to conclude that Ca-montmorillonite is more reactive. This is contrary to the conclusions presented by Taylor-Lange et al. [36], where a Na-bentonite/kaolin blend was considered to be more reactive than Ca-bentonite/kaolin blend. However, as mentioned previously, the kaolin content in these blends was varied as well, which would undoubtedly have an effect on reactivity.

No defined optimum temperature was reported for hectorite; however, the authors observed formation of crystalline phases starting at 800˚C. CH consumption also appeared to be unaffected by calcination temperature and was the lowest among all clay samples. The low reactivity of this clay was attributed to its low Al and high Mg content. It should be noted that the SiO_2+Al_2O_3+Fe_2O_3 content of hectorite was well below the 70.0% specified by ASTM C618.

For illite, the maximum amorphous content was observed at 900˚C, although a large portion of crystalline material was present as well. CH consumption was also highest at this temperature, although it was the second lowest after hectorite. Although the SiO_2+Al_2O_3+Fe_2O_3 content of the illite was above 70%, this value did not correlate well with calcined clay reactivity.

Danner et al. [37] assessed the performance of smectite-rich clay obtained from marine sediment (marl) and calcined at 600 - 1,000˚C. Dehydroxylation of small quantities of kaolinite was observed at 650˚C, while for smectite and illite, the dehydroxylation temperature was reported to be 800˚C. Compressive strength of mortars containing 20 and 35% of clay calcined at 800˚C was similar to that of OPC after 7 days. Unfortunately, the exact mineralogy of the clay, specifically the particular smectite minerals present, was not reported in this study. Therefore, it is difficult to compare the findings of Danner et al. [37] to other published results, as Hollanders et al. [45] clearly showed that calcined smectites have a wide range of reactivities.

1.4. Conclusions

Based on the review of current literature, the use of calcined natural clays in concrete as a cement-replacement material is a viable option. Clays containing kaolinite appear to be the most economical due to potentially lower calcination temperatures and being the most reactive. A wide range of calcination temperatures has been published for each clay type, especially for kaolin; therefore, the optimum calcination temperatures have to be determined for each clay individually.

Although it has been reported in the literature that reactivity of clays depends on their mineralogy, relative amounts of clay minerals present, particle size, degree of order/disorder (in the case of kaolinite), and the amount of associated minerals, the exact relationships between these parameters and reactivity have not been established. Moreover, the degree to which each parameter affects overall reactivity is not clear. Additionally, it has been shown in the literature that complete loss of crystallinity, as determined XRD, may not always correspond to maximum reactivity of the calcined material, especially in the case of kaolinite-containing clays. Currently, the most reliable predictor of reactivity appears to be compressive strength measurements. The use of isothermal calorimetry for this purpose has only been explored in one study that the authors are aware of.

1.5. References

[1] H. Justnes, “How to Make Concrete More Sustainable,” *J. Adv. Concr. Technol.*, vol. 13, no. 3, pp. 147–154, 2015.

[2] K. L. Scrivener, “Options for the future of cements,” *Indian Concr. J.*, vol. 88, no. 7, pp. 11–21, 2014.

[3] F. Bergaya and G. Lagaly, “General introduction: Clays, clay minerals, and clay science,” in *Developments in Clay Science*, vol. 1, F. Bergaya, B. K. G. Theng, and G. Lagaly, Eds. Elsevier Ltd., 2006, pp. 1–19.

[4] C. H. Zhou and J. Keeling, “Fundamental and applied research on clay minerals: From climate and environment to nanotechnology,” *Appl. Clay Sci.*, vol. 74, pp. 3–9, 2013.

[5] A. K. Chakraborty, *Phase Transformation of Kaolinite Clay*. New Delhi, India: Springer, 2014.

[6] C. Bich, J. Ambroise, and J. Péra, “Influence of degree of dehydroxylation on the pozzolanic activity of metakaolin,” *Appl. Clay Sci.*, vol. 44, no. 3–4, pp. 194–200, May 2009.

[7] R. Fernandez, F. Martirena, and K. L. Scrivener, “The origin of the pozzolanic activity of calcined clay minerals: A comparison between kaolinite, illite and montmorillonite,” *Cem. Concr. Res.*, vol. 41, no. 1, pp. 113–122, Jan. 2011.

[8] E. Badogiannis, G. Kakali, G. Dimopoulou, E. Chaniotakis, and S. Tsivilis, “Metakaolin as a main cement constituent. Exploitation of poor Greek kaolins,” *Cem. Concr. Compos.*, vol. 27, no. 2, pp. 197–203, 2005.

[9] N. Garg and J. Skibsted, “Pozzolanic reactivity of a calcined interstratified illite/smectite (70/30) clay,” *Cem. Concr. Res.*, vol. 79, pp. 101–111, 2016.

[10] C. He, E. Makovicky, and B. Osbæck, “Thermal stability and pozzolanic activity of calcined kaolin,” *Appl. Clay Sci.*, vol. 9, pp. 165–187, 1994.

[11] C. He, E. Makovicky, and B. Øsbæck, “Thermal stability and pozzolanic activity of calcined illite,” *Appl. Clay Sci.*, vol. 9, no. 5, pp. 337–354, 1995.

[12] C. He, B. Osbaeck, and E. Makovicky, “Pozzolanic Reactions of Six Principal Clay Minerals: Activation, Reactivity Assessments and Technological Effects,” *Cem. Concr.*

Res., vol. 25, no. 8, pp. 1691–1702, 1995.

[13] C. He, E. Makovicky, and B. Osbæck, “Thermal treatment and pozzolanic activity of Na- and Ca-montmorillonite,” *Appl. Clay Sci.*, vol. 10, no. 5, pp. 351–368, 1996.

[14] C. He, E. Makovicky, and B. Osbæck, “Thermal treatment and pozzolanic activity of sepiolite,” *Appl. Clay Sci.*, vol. 10, no. 5, pp. 337–349, 1996.

[15] C. He, E. Makovicky, and B. Osbæck, “Thermal stability and pozzolanic activity of raw and calcined mixed-layer mica/smectite,” *Appl. Clay Sci.*, vol. 17, no. 3–4, pp. 141–161, 2000.

[16] N. Amin, S. Alam, and S. Gul, “Assessment of pozzolanic activity of thermally activated clay and its impact on strength development in cement mortar,” *RSC Adv.*, vol. 5, no. 8, pp. 6079–6084, Dec. 2015.

[17] G. Kakali, T. Perraki, S. Tsivilis, and E. Badogiannis, “Thermal treatment of kaolin: the effect of mineralogy on the pozzolanic activity,” *Appl. Clay Sci.*, vol. 20, no. 1–2, pp. 73–80, Sep. 2001.

[18] L. Piga, “Thermogravimetry of a kaolinite-alunite ore,” *Thermochim. Acta*, vol. 265, no. C, pp. 177–187, 1995.

[19] H. Ghorbel and B. Samet, “Effect of iron on pozzolanic activity of kaolin,” *Constr. Build. Mater.*, vol. 44, pp. 185–191, 2013.

[20] S. Mohammed, “Processing, effect and reactivity assessment of artificial pozzolans obtained from clays and clay wastes: A review,” *Constr. Build. Mater.*, vol. 140, pp. 10–19, 2017.

[21] R. Snellings, G. Mertens, and J. Elsen, “Supplementary cementitious materials,” *Rev. Mineral. Geochemistry*, vol. 74, no. 1, pp. 211–278, Dec. 2012.

[22] E. Gasparini, S. C. Tarantino, P. Ghigna, M. P. Riccardi, E. I. Cedillo-Gonzalez, C. Siligardi, and M. Zema, “Thermal dehydroxylation of kaolinite under isothermal

conditions," *Appl. Clay Sci.*, vol. 80–81, pp. 417–425, 2013.

[23] B. Sabir, S. Wild, and J. Bai, "Metakaolin and calcined clays as pozzolans for concrete: a review," *Cem. Concr. Compos.*, vol. 23, no. 6, pp. 441–454, Dec. 2001.

[24] H. Rahier, B. Wullaert, and B. Van Mele, "Influence of the Degree of Dehydroxylation of Kaolinite on the Properties of Aluminosilicate Glasses," *J. Therm. Anal. Calorim.*, vol. 62, pp. 417–427, 2000.

[25] A. Teklay, C. Yin, L. Rosendahl, and M. Bøjer, "Calcination of kaolinite clay particles for cement production: A modeling study," *Cem. Concr. Res.*, vol. 61–62, pp. 11–19, 2014.

[26] S. Hollanders, *Mineralogical study of the pozzolanic properties of calcined clays*, University of Leuven, 2017.

[27] Y. Leng, *Materials Characterization: Introduction to Microscopic and Spectroscopic Methods*, 2nd ed. Singapore: Wiley-VCH, 2013.

[28] J. Ambroise, S. Maximilien, and J. Pera, "Properties of metakaolin blended cements," *Adv. Cem. Based Mater.*, vol. 1, no. 4, pp. 161–168, 1994.

[29] G. Batis, P. Pantazopoulou, S. Tsivilis, and E. Badogiannis, "The effect of metakaolin on the corrosion behavior of cement mortars," *Cem. Concr. Compos.*, vol. 27, no. 1, pp. 125–130, Jan. 2005.

[30] C.-S. Poon, L. Lam, S. . Kou, Y.-L. Wong, and R. Wong, "Rate of pozzolanic reaction of metakaolin in high-performance cement pastes," *Cem. Concr. Res.*, vol. 31, no. 9, pp. 1301–1306, Sep. 2001.

[31] W. Aquino, D. A. Lange, and J. Olek, "The influence of metakaolin and silica fume on the chemistry of alkali-silica reaction products," *Cem. Concr. Compos.*, vol. 23, pp. 485–493, 2001.

[32] T. Ramlochan, M. Thomas, and K. A. Gruber, "The effect of metakaolin on alkali–silica reaction in concrete," *Cem. Concr. Res.*, vol. 30, no. 3, pp. 339–344, Mar. 2000.

[33] N. M. Al-Akhras, “Durability of metakaolin concrete to sulfate attack,” *Cem. Concr. Res.*, vol. 36, no. 9, pp. 1727–1734, Sep. 2006.

[34] L. Courard, A. Darimont, M. Schouterden, F. Ferauche, X. Willem, and R. Degeimbre, “Durability of mortars modified with metakaolin,” *Cem. Concr. Res.*, vol. 33, no. 9, pp. 1473–1479, Sep. 2003.

[35] N. J. Coleman and C. L. Page, “Aspects of the Pore Solution Chemistry of the Hydrated Cement Pastes Containing Metakaolin,” *Cem. Concr. Res.*, vol. 27, no. 1, pp. 147–154, 1997.

[36] S. C. Taylor-Lange, E. L. Lamon, K. A. Riding, and M. C. G. Juenger, “Calcined kaolinite–bentonite clay blends as supplementary cementitious materials,” *Appl. Clay Sci.*, vol. 108, pp. 84–93, 2015.

[37] T. Danner, H. Justnes, G. Norden, and T. Østnor, “Feasibility of Calcined Marl as an Alternative Pozzolanic Material,” K. Scrivener and A. Favier in *Proceedings of the 1st International Conference on Calcined Clays for Sustainable Concrete*, RILEM Bookseries, vol. 10, Springer, Dordrecht, pp. 67–73, 2015.

[38] A. Tironi, M. A. Trezza, A. N. Scian, and E. F. Irassar, “Kaolinitic calcined clays: Factors affecting its performance as pozzolans,” *Constr. Build. Mater.*, vol. 28, no. 1, pp. 276–281, 2012.

[39] S. Krishnan and S. Bishnoi, “High Level Clinker Replacement in Ternary Limestone-Calcined Clay-Clinker Cement,” *Adv. Struct. Eng.*, pp. 1725–1731, 2015.

[40] R. Pierkes, S. E. Schulze, and J. Rickert, “Optimization of Cements with Calcined Clays as Supplementary Cementitious Materials,” K. Scrivener and A. Favier in *Proceedings of the 1st International Conference on Calcined Clays for Sustainable Concrete*, RILEM Bookseries, vol. 10, Springer, Dordrecht, pp. 59–66, 2015.

[41] A. Alujas, R. Fernández, R. Quintana, K. L. Scrivener, and F. Martirena, “Pozzolanic reactivity of low grade kaolinitic clays: Influence of calcination temperature and impact of

calcination products on OPC hydration," *Appl. Clay Sci.*, vol. 108, pp. 94–101, May 2015.

[42] K. E. Rasmussen, M. Moesgaard, L. L. Køhler, T. T. Tran, and J. Skibsted, "Comparison of the pozzolanic reactivity for flash and soak calcined clays in Portland cement blends," K. Scrivener and A. Favier in *Proceedings of the 1st International Conference on Calcined Clays for Sustainable Concrete*, RILEM Bookseries, vol. 10, Springer, Dordrecht, pp. 151–157, 2015.

[43] N. Beuntner and K. C. Thienel, "Properties of Calcined Lias Delta Clay—Technological Effects, Physical Characteristics and Reactivity in Cement," K. Scrivener K and A. Favier in *Proceedings of the 1st International Conference on Calcined Clays for Sustainable Concrete*, RILEM Bookseries, vol. 10, Springer, Dordrecht, pp. 43–50, 2015.

[44] N. Garg and J. Skibsted, "Thermal activation of a pure montmorillonite clay and its reactivity in cementitious systems," *J. Phys. Chem. C*, vol. 118, no. 21, pp. 11464–11477, 2014.

[45] S. Hollanders, R. Adriaens, J. Skibsted, O. Cizer, and J. Elsen, "Pozzolanic reactivity of pure calcined clays," *Appl. Clay Sci.*, vol. 132–133, pp. 552–560, 2016.

Chapter 2. Identification of the Local Clay Sources and Evaluation of Chemical and Mineral Composition

2.1. Introduction

The goal of this project is to obtain and assess various kaolinite content clays from the state of Florida to assess their potential for use as supplementary cementitious materials (SCMs). This report includes a qualitative and quantitative multi-technique characterization of the obtained clays using x-ray fluorescence (XRF), x-ray diffraction (XRD), and thermogravimetric analysis (TGA). A total of 20 clays with varying chemical and physical properties were obtained and analyzed. The collected clays had varying kaolinite ($Al_2Si_2O_5(OH)_4$) content, which is expected to play a significant role in the pozzolanic activity of calcined clay.

2.2. Assessing and Obtaining Florida Clay Samples

There is currently a plethora of available literature on most of the clay sources located across the state of Florida ([1]–[5]). Much of the characterization is focused on reporting the elemental oxide analyses rather than the clay mineralogy. Despite all the geological research published on Florida clay resources, the Florida Department of Environmental Protection has the most user-friendly and detailed database of clay resources in the state. This agency has put together a user-friendly program known as the Integrated Habitat Network (IHN), which includes a 2-D map of the many facets of Florida's natural and man-made geology, such as mining areas, hydrography, hazardous waste locations, natural habitats, parks and recreation, conservation areas, recreational parks, etc. [6]. The non-phosphate sites information (updated in 2016) provided by IHN was used to identify potential clay sampling locations. This data revealed that Florida clay sources may be found all across the state of Florida from the west side of the panhandle all the way across to east Florida in Jacksonville and as far south as Key Largo. It should be noted that although the IHN provides specific locations for clay, sand, limestone, fuller's earth, and fill material mining, these materials are mined with some proportions of clay. All non-phosphate locations on the IHN database were considered as potential sites for obtaining clay specimens. The database offered by the IHN is, however, somewhat limited. The non-phosphate resources shown in this program are not guaranteed to exist currently as they are listed. In addition, no specific information on the mineralogy of the clay sources is available within the IHN network. Other

resources were needed for the characterization of clays at these locations and proved difficult or impossible to obtain. Most of these locations are either active or inactive industrial mining operations. However, quite a few clay sources existed on private property and specimen gathering was limited to properties for which the owner's consent could be obtained.

This project focused on obtaining raw earth materials as they exist naturally in the ground. A total of 20 potential clays from 9 different clay pits were obtained for this project. All clay samples for this project were grab samples placed into 5-gallon plastic buckets. The detailed physical description of each clay sample is presented in this report.

A red overburden clay was obtained from a sand mining operation at a pit listed as Pit 168$\hat{A}$. This mine has high quality sand residing under 10-15 feet of overburden clay. Figure 2-1a, shows the reddish overburden at the top of the excavation. This overburden is currently used as a road base material. A Google Maps [7] image of the pit's layout is shown in Figure 2-1b [7].

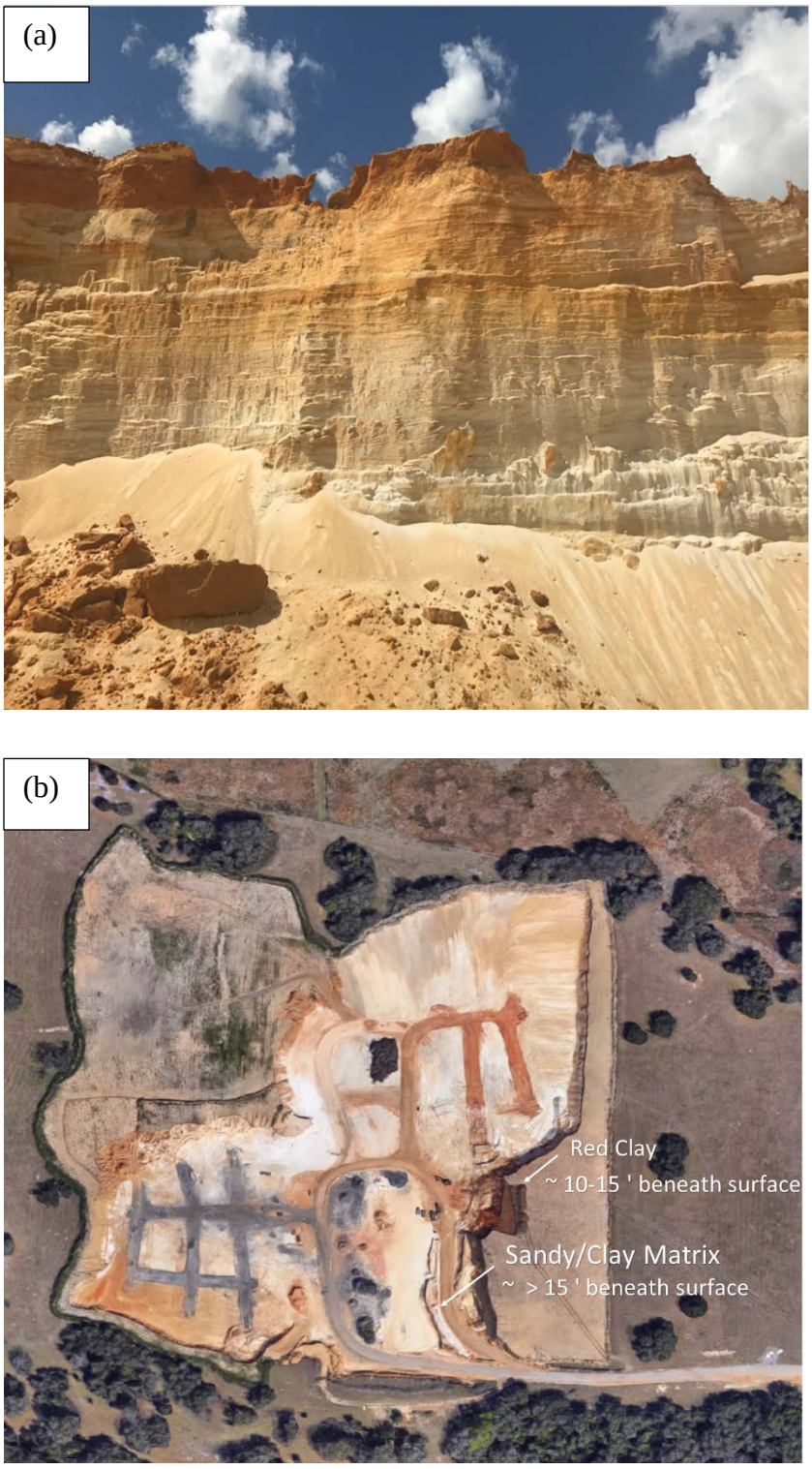

Figure 2-1: Clay Pit 168Â: (a) clay stratification in the mine wall, (b) aerial view [7]

Another overburden red clay was obtained from a mine (Figure 2-2) that is also excavated for sand; however, a red clay overburden as deep as 15 feet from the surface is excavated and sold for road/construction base material. The owner of the mine mentioned that there was white clay in the rear of the property, but would not aid in obtaining samples because of safety concerns.

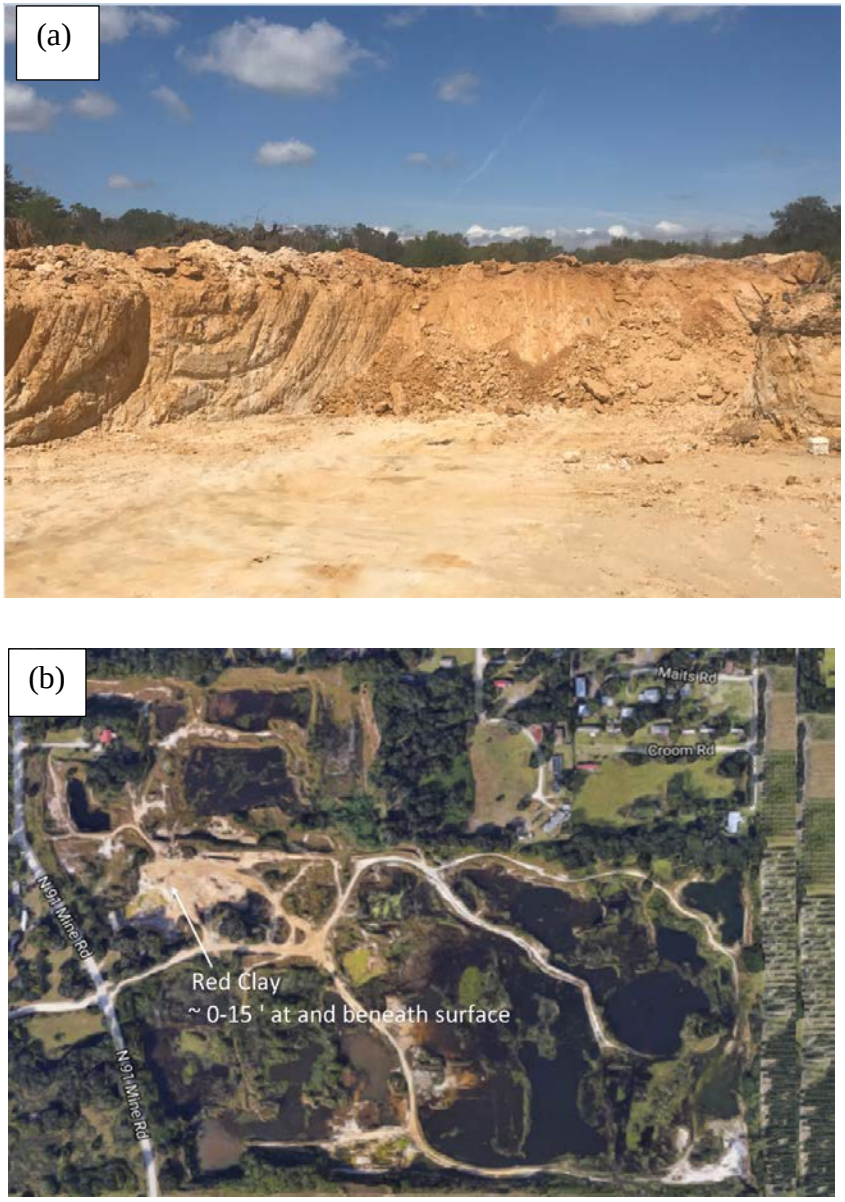

Figure 2-2: Clay Mine: (a) sample clay wall, (b) aerial view [7]

At another mine, large quantities of 2 types of clay are found up to 30 feet beneath the surface at 2 separate locations in the mine. One of the clays is sold as a fill material, and the other

clay is a plastic gray-colored clay that is sold for use as a water basin sediment densifier that aids bed sediments with water retention. An aerial view of the mine is shown in Figure 2-3. Excavation had not begun when this image was taken.

Figure 2-3: Clay Mine [7] with 2 types of clay

Several red clays were also obtained from another clay mining company that owns 11 properties, but most are not excavated for clay. Two mines were visited for sample grabbing. Cannon Pit is currently mined for high quality baseball clay. This clay is extremely dark red in color and is sold as a specialty clay. For this reason, this clay was not chosen for this project. Another mine named Pit #17 was also visited (Figure 2-4). This mine is currently inactive, but was previously mined for lower-quality red clay that can be sold as road/construction base. A sample of this clay was obtained for this study.

Figure 2-4: Clay Pit #17: (a) aerial view [7], (b) sample clay wall

Another clay source was found at a limestone mine (Figure 2-5) that has clay, contained in overburden excavated in the process of mining limestone, that has been set aside for sale as fill material or road/construction base. Large amounts of red clay are found 30 feet beneath the surface. In addition, a plastic gray clay known as Florida Gumbo is found sparsely among the red

clay deposits. There is also a very dark overburden material as deep as 10 feet beneath the surface, above the red clay, which is sold as fill. Samples of all three clays were obtained for this research project.

Figure 2-5: Limestone/Clay Mine [7]

Eight clay samples were obtained from different locations in a mine that produces both sand and red clay. Five different red clays were identified by visual inspection of the clay color. In addition, a black clay, a white sandy clay, and a white plastic clay were obtained. All clays were found in the mine up to 15 feet beneath the surface. The white plastic clay is typically avoided during mining operations due to the difficulty experienced in excavating the material from earth

due to its plasticity. In addition, it was noted that the black clay exists in very small quantities within the earth of the LLC mine and is not mined. An aerial view of the mine revealing each of the 8 clay locations is shown in Figure 2-6. It should be noted that only 3 of the 5 red clays obtained at this mine were used for this project; 2 of the five were not included because they had x-ray diffraction (XRD) patterns that were not different enough from the other 3 clays to warrant inclusion.

Figure 2-6: Clay Mine [7] containing 8 different clays

Access was obtained to a currently inactive clay mine that was previously mined for sand and red clay. Two red clay specimens were obtained from this mine, although only one was used

for this project since their XRD patterns were nearly identical. An aerial view of the mine is shown in Figure 2-7.

Figure 2-7: Inactive Clay Mine [7]

An active mine with 2 clay/sand mines containing high-purity kaolinite clay was visited. There is approximately 10 - 20 feet of overburden that must be removed to access high purity kaolinite containing white sandy clay. The clay is mined via dredging in water retention ponds as deep as 60 feet beneath the surface. Beneath the kaolin clay resides a grey, plastic montmorillonite clay previously mentioned as Florida Gumbo. The Florida Gumbo was not being mined due to issues with slurry generation for transport from the ground to the processing plant. Two overburden materials (one grey and the other orange in color), as well as a high-quality air-floated kaolinite clay (> 97 wt. % kaolinite) and Florida Gumbo clay were obtained from this clay mine. It is noted that the high-quality kaolinite was not used for this project, as lower quality clays with lower kaolinite contents are of primary interest for this research. An aerial view of the mine is shown in Figure 2-8, while images of the overburden materials and dredging operation are included in Figure 2-9.

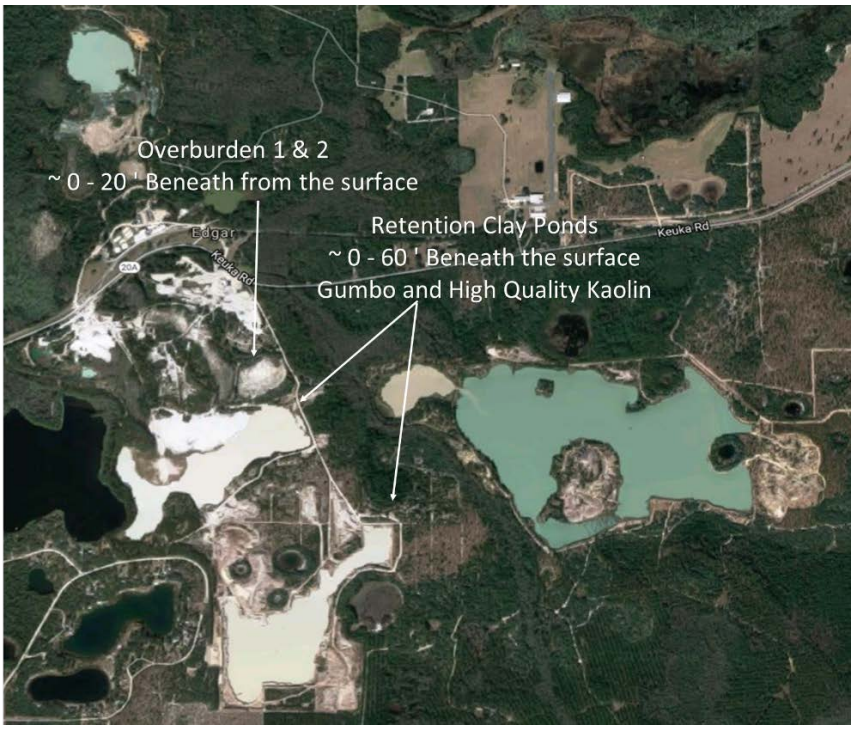

Figure 2-8: High Purity Kaolin Mine, aerial view [7]

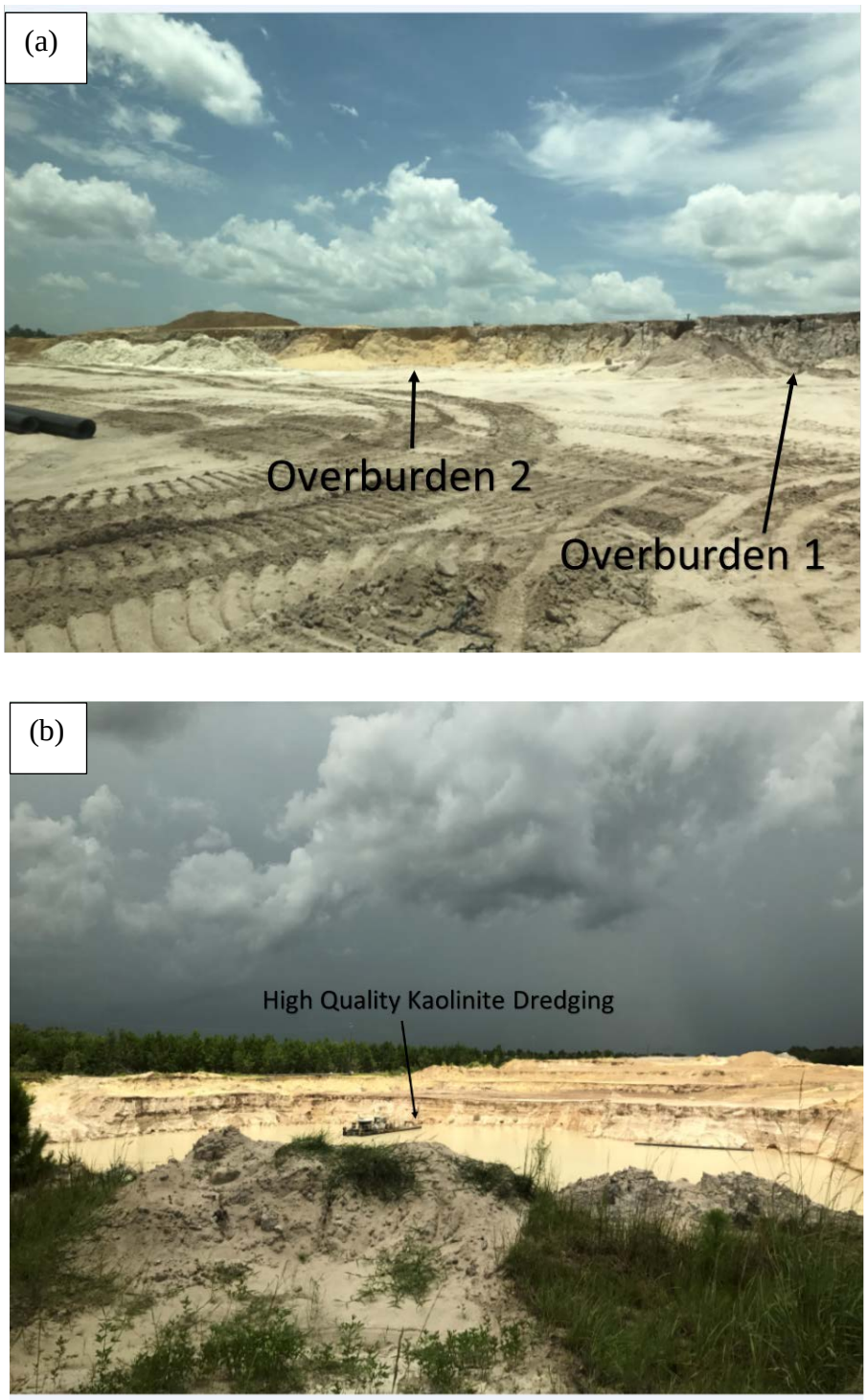

Figure 2-9: High Purity Kaolin Mine: (a) overburden materials, (b) dredging operation

A second high-quality kaolinite mine is currently inactive and the owner has no current interest in starting up the mine. Two white sandy clays were obtained from this mine, one from

the high-quality kaolin source roughly 20 feet beneath the surface, and the other from the overburden roughly 10 - 15 feet beneath the surface and above the high-quality kaolinite clay. An aerial view of the mine is shown in Figure 2-10.

Figure 2-10: Second High-Purity Kaolin Mine [7]

2.3. Characterization of the Obtained Samples

A total of 20 samples were obtained from the field as described in Section 2.2. In the laboratory, each sample was spread out on the floor, crushed by hand, and mixed thoroughly. After mixing, all clays were dried in a Lindberg box furnace at 110°C until a constant mass was achieved.

After drying, each sample was sieved through a 325-mesh (45-μm) sieve to separate the clay size fraction from the large quantities of sand present in each sample. A preliminary evaluation of the material passing the 45-μm sieve was carried out using XRD in order to identify samples for detailed characterization. XRD scans were collected using a Phillips X'Pert PW3040 Pro diffractometer equipped with an X'Celerator Scientific detector and a Cu-Kα x-ray source. Tension and current were set to 45 kV and 40 mA, respectively; 5-mm divergence and anti-scatter

slits were used in the automatic mode. Scans were collected for the 4-70˚ 2θ angular range, and the sample was rotated at 30 rpm during data collection. The collected diffraction patterns were compared to one another using the HighScore Plus v. 4.5 software in order to identify the samples' mineralogies. For samples with very similar x-ray diffraction patterns, only one sample was selected. Based on this examination, 11 samples were identified for further study.

2.4. Sand Content Determination

For the selected 11 samples, approximately 1 kg each of dried material was weighed out and wet-sieved through a 45-μm sieve. The materials retained and passing the 45-μm sieve were dried again at 110°C in a box oven until a constant mass was attained. It should be noted that surface water, internally-adsorbed water, and chemical water may still persist in each clay after drying at 110°C. The percentage retained on the 45-μm sieve was considered to be the sample's sand content, and the percentage passing was taken as the sample's clay content. Table 2-1 shows that sand content in all the samples was high, ranging from approximately 65% to 80%, which is well above the maximum 34% specified by ASTM C618 [8]. Correspondingly, the clay content varied from 35% to 20%.

Table 2-1: Sand and clay content characterization determined by wet sieve analysis

Sample ID	% Retained on 45-μm Sieve (Sand wt. %)	% Passing 45-μm Sieve (Clay wt. %)
A1	77.0	23.0
A2	75.9	24.1
B1	67.4	32.6
B2	81.2	18.8
B3	75.1	24.9
B4	73.5	26.5
C	79.9	20.1
D1	64.8	35.2
E	89.5	10.5
F	76.4	23.6
G	75.2	24.8

2.5. Elemental Oxide Composition

After wet sieving, the material was oven dried at 110°C for further elemental analyses. The compositions of the clay fraction (passing the 45-μm sieve) were determined using XRF according to ASTM C114 [9]. Since the fraction retained on the 45-μm sieve was visually classified as quartz sand, XRF analysis was not conducted on the retained material.

As can be seen from Table 2-2, the clay fraction consisted predominantly of Al_2O_3 (30 - 38%) and SiO_2 (34 - 46%), which is generally consistent with the chemical composition of kaolinite ($Al_2O_3 \cdot 2SiO_2 \cdot 2H_2O$, 39.5 wt% Al_2O_3, 46.5 wt% SiO_2, and 14.0 wt% H_2O). The high loss on ignition content (LOI) was assumed to be due to the water chemically combined in kaolinite (14.0 wt%), which would be lost during the calcination process. Fe_2O_3 content of the clay fractions varied from approximately 1 to 10%. Increase in Fe_2O_3 content generally corresponded to an increase in the red color of the clay. All the clays met the ASTM C618 [8] requirement of a minimum of 70.0% for $SiO_2+Al_2O_3+Fe_2O_3$. Additionally, the SO_3 content of all the clays was very low, below 0.1 %, which was well below the maximum limit of 4% specified by ASTM C618 [8]. However, it should be noted that although the clay fraction of the obtained field samples met the requirements of ASTM C618 [8], the bulk material would not meet this specification due to its large sand content in the as-received condition unless it was first ground to pass a 325-mesh sieve.

Table 2-2: Oxide chemical composition of the clay fraction

Clay ID	A1	B2	B3	B4	B1	C	D1	F	E	G
Analyte	wt.%	wt.%	wt.%	wt.%	wt.%	wt.%	wt.%	wt.%	wt.%	wt.%
SiO_2	45.99	43.32	37.07	41.09	42.52	34.05	38.47	42.63	43.67	43.84
Al_2O_3	37.7	34.33	33.11	33.31	35.88	33.13	31.29	34.94	30.08	32.52
Al_2O_3/ SiO_2	0.820	0.792	0.893	0.811	0.844	0.973	0.813	0.820	0.689	0.742
Fe_2O_3	0.9	2.99	10.2	5.35	1.63	6.58	8.91	4.55	6.52	5.48
CaO	< 0.01	< 0.01	0.02	0.17	0.05	1.1	0.12	< 0.01	0.37	< 0.01
MgO	0.16	0.24	0.34	0.33	0.39	0.29	0.49	0.21	0.28	0.22
SO_3	< 0.01	< 0.01	< 0.01	< 0.01	< 0.01	0.06	< 0.01	< 0.01	0.02	< 0.01
Na_2O	0.05	0.04	0.05	0.05	0.03	0.23	0.05	0.02	0.02	0.02
K_2O	0.24	0.18	0.15	0.15	0.18	0.24	0.23	0.12	0.17	0.3
TiO_2	0.27	2.52	1.5	1.69	1.52	1.05	1.39	1.13	1.76	1.18
P_2O_5	0.05	0.4	0.77	1.12	0.66	5.39	1.26	0.21	0.27	0.81
Mn_2O_3	< 0.01	< 0.01	0.01	0.01	< 0.01	< 0.01	0.01	< 0.01	0.01	0.01
SrO	< 0.01	0.08	0.12	0.18	0.12	0.49	0.16	0.04	0.03	0.23
Cr_2O_3	< 0.01	0.01	0.03	0.02	0.02	0.043	0.03	0.02	0.02	0.01
ZnO	< 0.01	< 0.01	< 0.01	< 0.01	< 0.01	< 0.01	< 0.01	< 0.01	< 0.01	< 0.01
BaO	< 0.01	0.06	0.07	0.1	0.07	0.25	0.09	0.01	0.02	0.16
L.O.I (950˚C)	14.17	15.06	16.52	15.56	16.14	16.33	16.6	15.39	15.66	14.41
Total	99.53	99.23	99.95	99.13	99.21	99.23	99.08	99.27	98.9	99.21
Na_2O_{eq}	0.21	0.16	0.15	0.15	0.15	0.38	0.2	0.1	0.14	0.22

2.6. Mineralogical Analysis

After separating the dry materials into clay and sand fractions, the clay fraction (passing the 45-μm sieve) was analyzed by XRD and TGA to determine its mineralogical composition.

2.6.1. X-ray Diffraction

X-ray diffraction (XRD) measurements were conducted in accordance with ASTM C1365 [10]. The external standard method was selected for determining the amorphous/unidentified content of the clay samples. Corundum (Standard Reference Material 676a) obtained from the

National Institute of Standards and Technology (NIST) was used as the external standard. The mass absorption coefficient (MAC) of corundum was 30.91 cm^2/g. MAC values for the clays were calculated based on their respective chemical oxide compositions listed in Table 2-2. Loss on ignition content was attributed to release of water. For the A2 sample, an internal standard method was used because XRF analysis was not done for this clay. 10% of corundum was added to the sample and mixed by hand with mortar and pestle to prevent the destruction of clay phases.

XRD scans were collected using the same procedures as described in Section 2.3. Moore and Reynolds [11] recommend the back-loading method for quantitative XRD analysis of clays, stating that "there seems to be little difference in the degree of randomness achieved between the complex and the simple methods." Therefore, the back-loading technique was used for placing all the samples into the sample holder in order to minimize preferred orientation. A number of clay sample preparation techniques have been suggested in the literature to achieve randomly-oriented particle packing ([11], [12]), most of which consist of clay deposition onto a zero-background plate. However, the resulting film typically cannot satisfy the infinite sample thickness assumption and therefore cannot be used for quantitative analysis ([11], [13]).

Phase identification and Rietveld refinement were performed using the PANalytical HighScore Plus 4.5 software [14]. Several approaches for Rietveld analysis have been proposed in the literature that yield good results for cementitious materials ([15]–[18]). However, refinement and quantification of natural clays is more complicated due to the varying degree of disorder of the kaolin group minerals. The kaolin group includes kaolinite, dickite, and nacrite, which are polytypes that differ in the stacking of the layers, and halloysite, which is a polymorph of kaolinite with additional water molecules incorporated into the crystal structure [19]. Brigatti et al. [19] state that the varying degree of disorder "commonly observed in kaolin minerals may be explained in terms of a series of stacking faults or defects" in the crystal structure. Additionally, the authors state that "this feature accounts for the well-known tendency of kaolin minerals to form a wide variety of ordered and disordered polytypes as well as twins," where several types of stacking can be observed in the same material. Russel and Fraser [20] also suggest that disorder could be due to a "small amount of dickite- and/or nacrite-like stacking in the kaolinite structure." Dickite- and nacrite-like stacking in low crystallinity kaolinites has been reported by Prost et al. [21], based on observed changes in the IR spectra of these materials at temperatures ranging from 5 to 600 K. As

the degree of disorder increases, peaks observed in the XRD diffraction patterns of kaolin group minerals become broader and more asymmetrical [19], making it increasingly challenging to obtain a good fitting through Rietveld refinement. It was observed in the current study that fitting of the clay XRD patterns, regardless of the degree of order/disorder, could be significantly improved when the kaolin content of the sample was considered to be equal to the sum of the kaolinite (ICSD 63192), dickite (ICSD 52398) and nacrite (ICSD 80083). In addition to variability in stacking, kaolinite can have a variable amount of isomorphous substitution of Al^{3+} in its crystal structure by Fe^{3+}, Mg^{2+}, Ti^{4+}, and V^{3+} [19], which can affect the quantification of this phase ([22], [23]). Since the amount of MgO and TiO_2 identified by XRF was low compared to Fe_2O_3 (Table 2-2), and vanadium was not detected, only Fe^{3+} substitution was considered in this study. A general formula of $(Al_2O_3)_{(1-x)}(Fe_2O_3)_x(SiO_2)_2(H_2O)_2$, was adopted for kaolinite, where *x* was the Fe-Al substitution parameter for all kaolin group phases. Refinement of Fe^{3+} substitution in the kaolinite structure during Rietveld analysis has been previously implemented by Prandel et al. ([22], [23]). The authors [22] pointed out that substitution of Fe^{3+} for Al^{3+} results in an increase in the unit cell volume of the kaolinite structure.

The following parameters were refined during Rietveld analysis in the current study: scale factors, lattice parameters, zero shift, fifth-order regular polynomial for background fitting, preferred orientation for all kaolin group phases in the (001) direction, peak shape parameters *w*, coordinates of atoms, and the Fe-Al substitution parameter *x*. The value of the substitution parameter, *x*, was controlled by comparison of the amount of the main oxides, SiO_2, Al_2O_3, and Fe_2O_3, determined by the Rietveld analysis, with that of the XRF analysis. The collected and fitted patterns for the B4 sample are shown in Figure 2-11 as an example.

It can be seen from Table 2-3 that the total kaolin content in the selected samples ranged from approximately 70 to 94 wt.%. All these clays are expected to have high reactivity on calcination due to their high kaolin contents. Hematite was identified in all the clays, except A1, A2, and B1, and was responsible for their red color. Small amounts of quartz were also detected in the clay fractions, ranging from 0.4 to 3.8%, except for clay E, where the amount of quartz was 10.3%. The amorphous/unidentified content of the samples may be due to the presence of allophane, which is a general name for amorphous, hydrous aluminosilicates commonly found in natural clays ([20], [24], [25]).

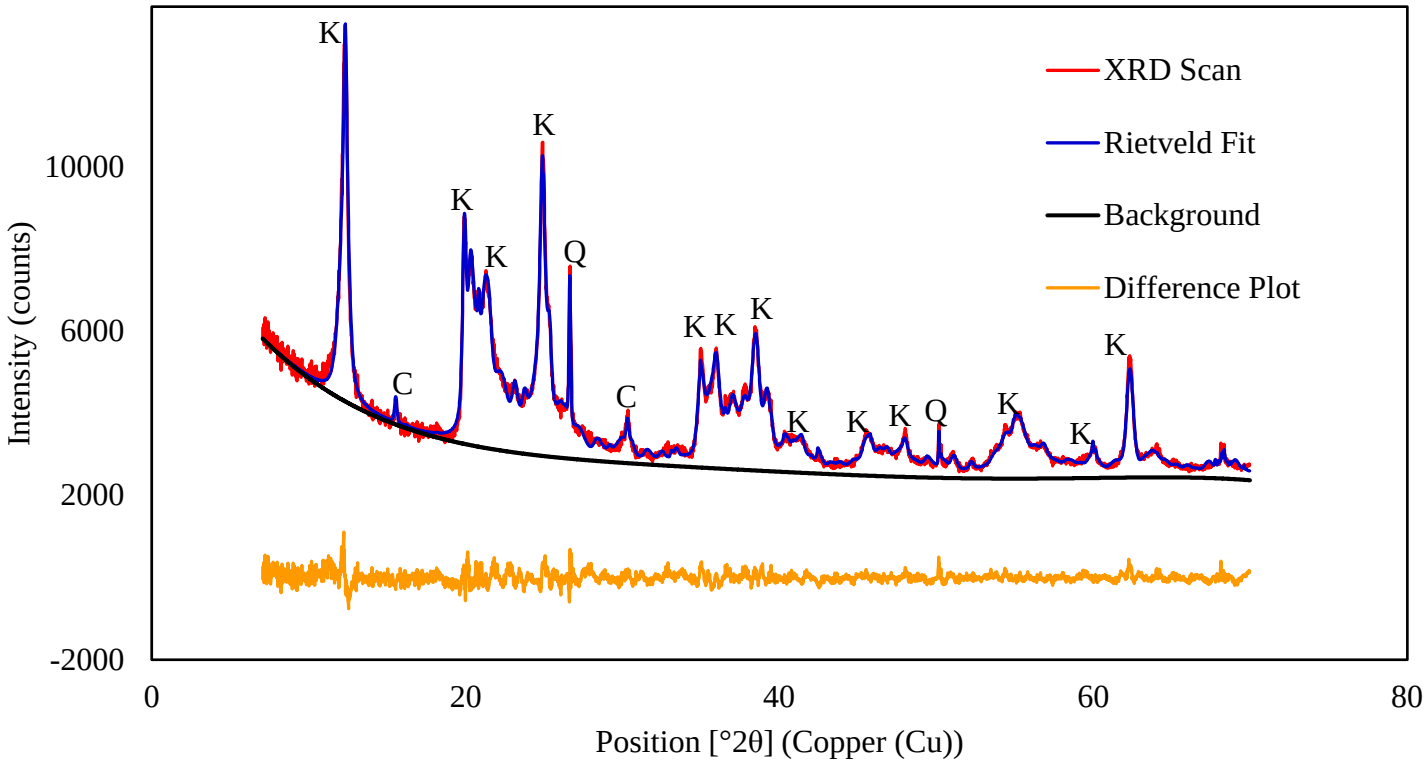

Figure 2-11 Rietveld refinement of B4 clay fraction. K = kaolinite, nacrite and dickite, C = crandallite, and Q = quartz.

Table 2-3: Results of Rietveld analysis of the sieved clays

	A1	A2	B1	B2	B3	B4	C	D1	E	F	G
Kaolinite (wt.%)	59.5	73.9	49.4	57.9	54.4	41.0	49.7	51.8	51.4	62.6	55.6
Nacrite (wt.%)	9.9	9.3	14.1	9.0	17.7	18.1	10.2	10.6	12.4	12.8	11.9
Dickite (wt.%)	20.2	10.5	23.9	17.6	11.2	23.0	10.4	16.0	7.6	10.5	10.2
Sum (Kaolin wt.%)	**89.6**	**93.7**	**87.4**	**84.5**	**83.3**	**82.1**	**70.2**	**78.4**	**71.4**	**85.9**	**77.7**
Fe^{3+} Substitution, *x*	0.00341	0.0	0.0128	0.0473	0.1874	0.0694	0.00538	0.1543	0.0130	0.0147	0.0310
Illite (wt.%)	0.6										
Crandallite (wt.%)			1.0	0.8	1.0	1.2	2.6	1.5	0.5	0.1	0.9
Hematite (wt.%)				0.5	0.7	0.1	0.4	0.1	1.0	1.0	1.4
Gibbsite (wt.%)							1.3		3.3		
Anatase (wt.%)			1.1	1.6	1.1	1.2	0.7	1.0	0.9	0.8	0.8
Quartz (wt.%)	1.7	2.7	0.4	1.9	1.2	2.0	0.6	2.4	10.3	1.5	3.8
Amorphous (wt.%)	8.2	3.6	10.2	10.7	12.7	13.5	24.2	16.6	12.5	10.8	15.4

2.6.2. Thermogravimetric Analysis

In addition to XRD, TGA measurements were performed on the clay fractions of the selected samples. TGA, unlike XRD, does not rely on the degree of crystallinity for mineral quantification, and it was used as a complimentary technique for the quantification of kaolin content. Additionally, TGA can be used to follow phase transformation of the clay minerals on heating, and can therefore be instrumental in selecting the appropriate calcination procedure.

TGA measurements were performed at the University of South Florida (USF) using an SDT Q600 series simultaneous TGA/differential scanning calorimeter (DSC) manufactured by TA Instruments. Approximately 5 mg of each sample was scanned in an open platinum crucible, under an inert nitrogen atmosphere, and using a constant heating rate from room temperature to 1000°C. It has been indicated in the literature that the heating rate can have a significant effect on the observed dehydroxylation temperatures and resolution [26]. Clay dehydroxylation can be identified on a TGA thermogram by a relatively sharp weight loss in the range of 300 - 900°C ([27]–[32]), as can be seen in Figure 2-12. Therefore, three heating rates of 5, 10, and 20°C/min were initially compared for A1 clay and are shown in Figure 2-12. As expected, an increase in the heating rate shifted the dehydroxylation temperatures to higher values, but the initial and final weight percentages were very similar. Since all three heating rates produced similar results, the heating rate of 20°C/min was selected and used for all the samples.

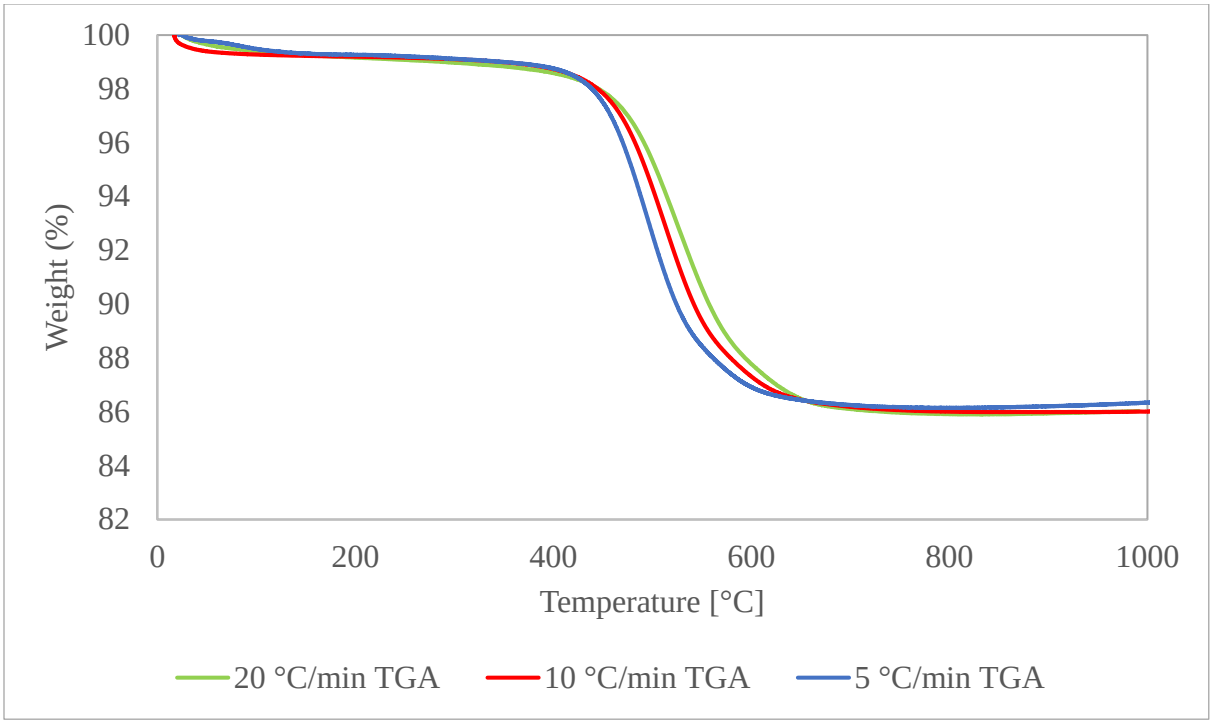

Figure 2-12: Comparison of the heating rates for the A1 clay

As recommended by [26], a derivative of the weight loss data was taken to improve resolution. This differentiation of thermogravimetric results is referred to as differential thermogravimetry (DTG), an example of which is shown in Figure 2-13. In the DTG curve, the dehydroxylation of kaolinite is characterized by a large endothermic peak which corresponds to the loss of structural water. DTG was used to identify the beginning and end of dehydroxylation period. It is widely accepted that kaolin group minerals: kaolinite, nacrite, and dickite undergo dehydroxylation between 450˚C - 600°C, depending on particle size and degree of disorder of kaolinite, as well as measurement conditions [31]. It can be observed in Figure 2-13 that all dehydroxylation of clay minerals was completed by approximately 650°C.

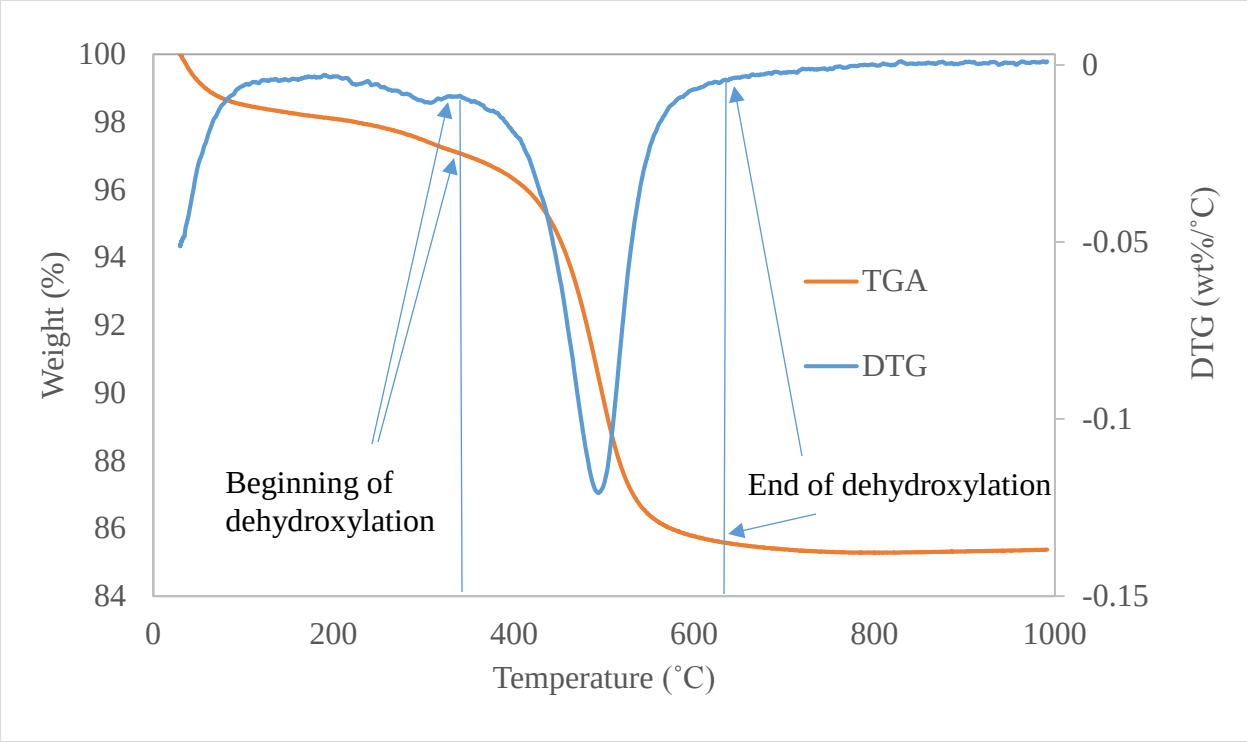

Figure 2-13: Example of thermogravimetric analysis and differential thermogravimetry curves

In addition to identifying the temperatures of the dehydroxylation period, the TGA curve was used to quantify the amount of kaolin in each clay sample. Two TGA quantification methods were considered: tangential and stepwise. In the stepwise method, the mass at the end of the dehydroxylation period is subtracted from the mass at the beginning of dehydroxylation period [26]. Although this method is convenient and easy to use, it does not take into account the mass loss coming from other minerals that may also be occurring at the beginning or end of the dehydroxylation period. The tangential method takes this into consideration by drawing a tangent line at the onset, offset, and point at which the rate of the thermal event is occurring most rapidly. The intersection of these tangents then becomes the temperature range used to compute the weight loss due to a specific thermal event. By using these intersecting tangents, a reduced weight loss due to a thermal event is observed if more than one thermal event is occurring at the temperature of onset or offset. This method results in a more accurate TGA quantification of clay minerals, since some minerals are seen to decompose within overlapping temperature intervals [33]. The tangential method was used for quantification of clay minerals as illustrated in Figure 2-14.

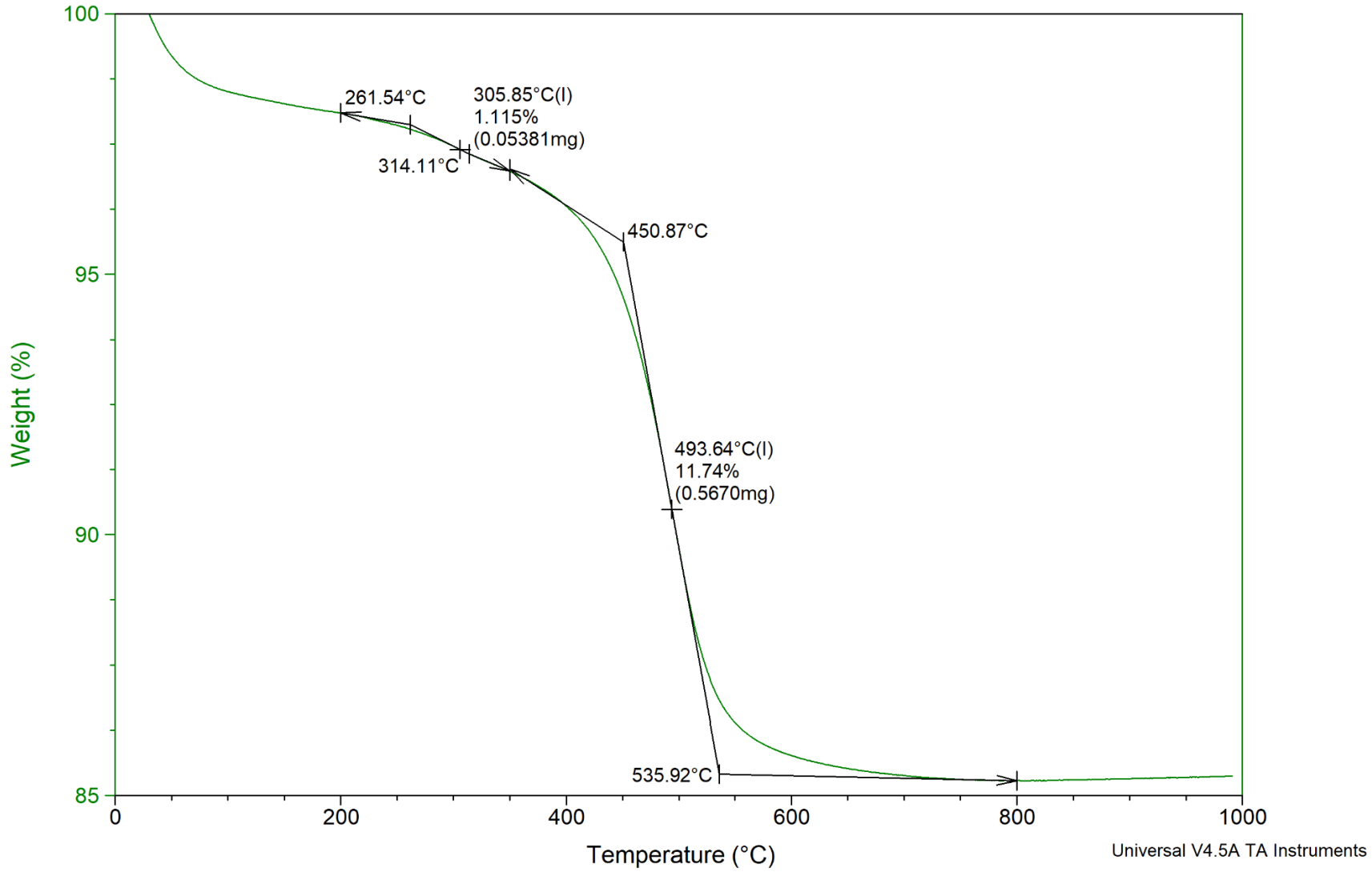

Figure 2-14: Illustration of the tangent method

TGA and DTG curves for all the samples are listed in Appendix A. Most of the clays showed mass loss events occurring in the temperature range of 200 - 350°C. These mass losses were quantified using the tangential method functionality of the TA Universal Analysis software by TA Instruments, and are listed in Table 2-4. This phenomena could possibly result from dehydroxylation of metal hydroxides such as gibbsite and iron oxyhydroxides or from the evaporation of adsorbed water in the presence of clay minerals ([27], [29], [34]). Although the presence of gibbsite and hematite was identified by XRD in the samples with mass loss in the range of 200 - 350°C, the maximum mass loss in Table 2-4 was greater than the maximum water content of these minerals (Table 2-3). Therefore, it appears that at least part of this mass loss was due to evaporation of strongly adsorbed water. Hence the mass loss in the temperature range of 200 - 350°C was reported as weight percent and not ascribed to any specific mineral or set of minerals. The weight loss reported was normalized to the mass of sample at 110°C after all residual free water was removed.

Table 2-4: Mass loss in the range of 200°C-350°C

Clay ID	Mass Loss (wt.%)
A1	0.0
A2	0.0
B1	0.0
B2	0.6
B3	2.1
B4	1.2
C	3. 3
D1	2.0
E	1.6
F	1.0
G	0.4

Since the weight loss during kaolin dehydroxylation is due to the loss of water, it is possible to calculate the amount of kaolinite in the sample using Equation 1:

$$m_K = m_{loss} \frac{M_K}{2M_{H_2O}} \qquad \text{Equation 1}$$

where m_K is the mass of theoretically-dehydroxylated, pure (no ion substitution) kaolin group minerals , m_{loss} is the TGA-determined mass loss over some temperature interval using the tangential method, M_K is the molecular mass of pure kaolin group minerals with no ion substitution (258.13 g/mol), M_{H_2O} is the molecular mass of water (18.0 g/mol), and the constant 2 corresponds to the 2 moles of water molecules chemically bound to one mole of a kaolin group mineral ($Al_2Si_2O_5(OH)_4$) [35]. The kaolinite formula was modified as discussed in Section 2.5 to account for iron substitution, which has a measurable effect on kaolinite molar mass.

Avet et al. [36] reported using a fixed temperature range of 400 - 600°C to quantify kaolinite content in their sample. However, it was observed in this study that the onset of the kaolinite dehydroxylation period varied somewhat between the samples, possibly indicating a variability in the degree of disorder. Therefore, the onset of dehydroxylation was identified as a minimum in the DTG curve between 300 and 400°C. The end of the dehydroxylation period was taken as 600°C for all the samples since no additional mass loss occurred between 650 and 800°C. The tangent method was used to determine the mass loss for each sample using the TA Universal Analysis software. The kaolinite content was then calculated using Equation 1. The results of this calculation are listed in the second column of Table 2-5.

As discussed in Section 2.5, iron can substitute for aluminum in the kaolinite structure. Therefore, for applicable comparison of the TGA and XRD analysis results, the kaolinite content determined by TGA was corrected to account for the amount of iron as shown in Table 2-3. The kaolinite content with no substitutions in Table 2-5 was recalculated using Equation 2 to account for the difference in molecular weight of kaolinite with incorporation of iron:

$$m_K(x) = m_K\left[1 + x\frac{M_{Fe_2O_3} - M_{Al_2O_3}}{M_K}\right] \qquad \text{Equation 2}$$

where $M_{Fe_2O_3} = 159.69$ g/mol and $M_{Al_2O_3} = 101.96$ g/mol are the molecular weights of iron and aluminum oxides, respectively. The corrected TGA quantification of kaolinite incorporating iron substitution, estimated using XRD analysis, is shown in the third column in Table 2-5. These results are in good agreement with those obtained by the XRD Rietveld analysis (Table 2-3).

Table 2-5: Kaolinite quantification using TGA tangential method

Clay ID	Kaolinite Content (wt.%) (no substitution)	Corrected Kaolinite Content (wt%) (with Fe substitution)	Difference in Kaolinite Content between XRD and TGA
A1	94.3	94.4	-4.8
A2	90.5	90.5	3.2
B1	90.9	91.1	-3.8
B2	79.2	80.1	4.4
B3	75.5	78.7	4.5
B4	82.2	83.5	-1.5
C	75.2	75.3	-5.1
D1	73.9	76.5	1.8
E	76.6	76.8	-5.4
F	86.2	86.5	-0.6
G	79.8	80.4	-2.5

In addition to TGA, DSC measurements were carried out for four of the 11 clay samples at the Florida Department of Transportation State Materials Office (SMO) because the instrument at USF was only capable of reaching a maximum temperature of 1000°C. The SDT Q600 series simultaneous TGA/ DSC manufactured by TA Instruments was used for the DCS measurements with the same settings as for TGA measurements, except that the maximum temperature was increased to 1500°C. A DSC can measure heat flow resulting from phase transitions, such as glass transitions, which are not accompanied by mass change and would not be detected by TGA [26].

DSC was used to evaluate the potential presence of amorphous silica in the samples. Amorphous silica can lead to concrete deterioration due to alkali aggregate reaction (AAR) [37]. It has been reported in the literature that amorphous silica is converted to cristobalite around 1200˚C [38]. As can be seen in Figure 2-15, a small peak around 1200˚C was observed in clay B4 only. The peaks between 900 and 1000˚C were attributed to precipitation of spinel and mullite, which are known to crystalize at 925˚C and 1050˚C respectively [38]. The peak between 400 and 600˚C was due to kaolinite dehydroxylation.

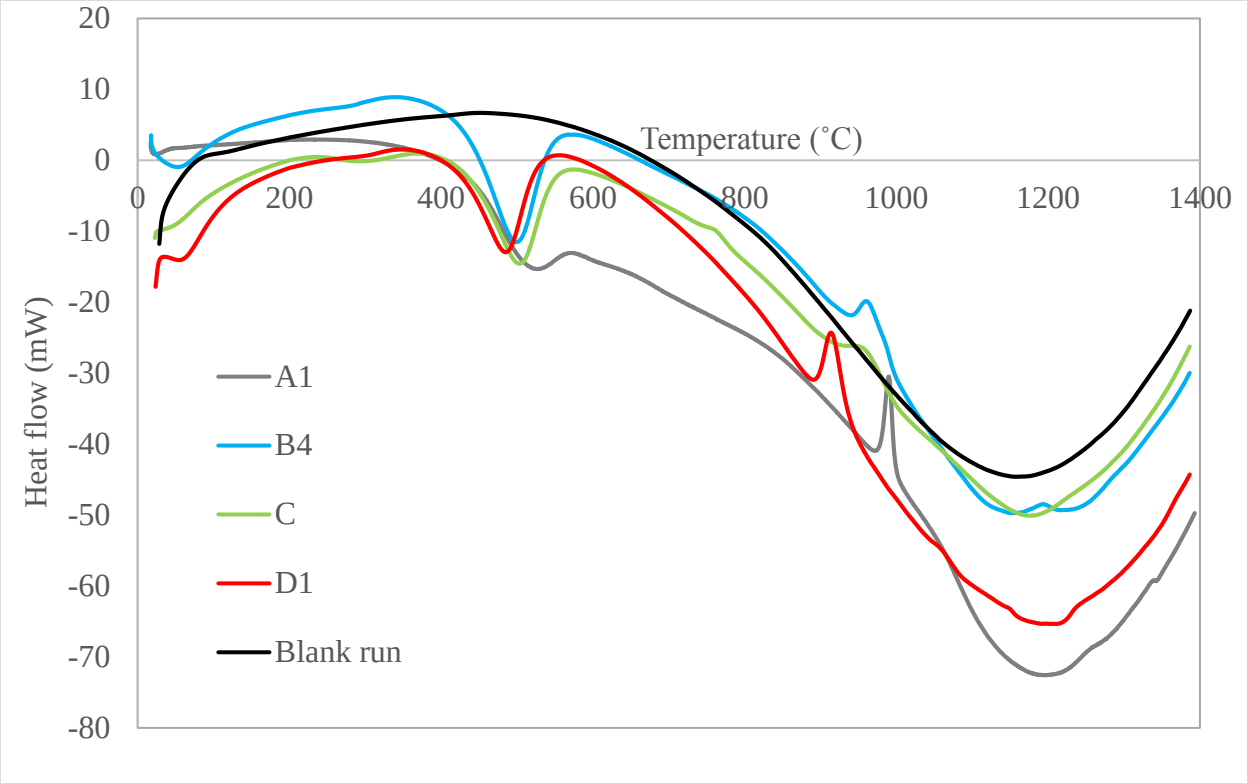

Figure 2-15: DSC heat flow curves for an empty crucible (blank run), A1, B4, C, and D1 clay samples

2.7. Conclusions

Field samples were obtained from 20 potential clay sources identified in the state of Florida. After preliminary characterization with XRD, 11 samples were selected for further quantification. The samples were wet-sieved on the 45-µm sieve to separate the predominantly clay material passing through from the predominantly sand material that is retained. ASTM C618 limits the amount retained on the sieve (greater than 45 µm) to a maximum of 34%. The amount retained ranged from approximately 65 to 80%, indicating that these materials must be beneficially processed before they can comply with ASTM C618. The fraction finer than 45 µm met the C618 chemical oxide composition requirements: minimum of 70.0% for SiO_2+Al_2O_3+Fe_2O_3 and SO_3 content of less than 4%. The kaolin content of the minus 325-mesh material was determined by XRD and TGA analyses and ranged from approximately 70 to 90%, indicating a good potential for producing a high-quality pozzolanic material on calcination. This material will certainly need

to be further evaluated in terms of long-term durability prior to its implementation and use as a supplementary cementitious material.

2.8. References

[1] J. L. Calver, *Florida Kaolins and Clays*, Tallahassee: Florida Geological Survey, 1949.

[2] John W. Hosterman and Sam H. Patterson, *Bentonite and Fuller's Earth Resources of the United States*, Washington: U.S. Geological Survey 1992.

[3] G. C. Matson, *Clays of Florida*, 1908.

[4] The Southeastern Geological Society, *Ochlocknee Mine and Little River Mine*, Tallahassee, 2013.

[5] Ernest, W. Bishop, a Lawrence L. Dee, Jr., *Guide to Rocks and Minerals of Florida*. Tallahassee: Florida Bureau of Geology, 1961.

[6] Florida Department of Environmental Protection, "Map Direct: Integrated Habitat Network (IHN)." [Online]. Available: https://ca.dep.state.fl.us/mapdirect/. [Accessed: 01-Jan-2017].

[7] Google Maps. (2017). *Google Maps*. [online], Available at: https://www.google.com/maps [Accessed Feb. 2017].

[8] ASTM Standard C618-12a, *Standard Specification for Coal Fly Ash and Raw or Calcined Natural Pozzolan for Use in Concrete*, West Conshohocken, PA: ASTM International, 2014.

[9] ASTM C114-13, *Standard Test Method for Chemical Analysis of Hydraulic Cement*, West Conshohocken, PA: ASTM International, 2013.

[10] ASTM C1365-06 (2011), *Standard Test Method for Determination of the Proportion of Phases in Portland Cement and Portland-Cement Clinker Using X-Ray Powder Diffraction Analysis*, West Conshohocken, PA: ASTM International, 2016.

[11] D. M. Moore and R. C. Reynolds, *X-ray Diffraction and the Identification and Analysis of*

Clay Minerals. New York, NY: Oxford University Press, 1989.

[12] A. K. Chakraborty, *Phase Transformation of Kaolinite Clay*. New Delhi, India: Springer, 2014.

[13] S. J. Chipera and D. L. Bish, "Baseline studies of the clay minerals society source clays: Powder X-ray diffraction analyses," *Clays Clay Miner.*, vol. 49, no. 5, pp. 398–409, 2001.

[14] "HighScore Plus v4.5." PANalytical B.V., Almelo, The Netherlands, 2016.

[15] R. Snellings, A. Bazzoni, and K. Scrivener, "The existence of amorphous phase in Portland cements: Physical factors affecting Rietveld quantitative phase analysis," *Cem. Concr. Res.*, vol. 59, pp. 139–146, May 2014.

[16] G. Álvarez-Pinazo, A. Cuesta, M. García-Maté, I. Santacruz, E. R. Losilla, A. G. De La Torre, L. León-Reina, and M. A. G. Aranda, "Rietveld quantitative phase analysis of Yeelimite-containing cements," *Cem. Concr. Res.*, vol. 42, no. 7, pp. 960–971, 2012.

[17] G. Le Saoût, V. Kocaba, and K. Scrivener, "Application of the Rietveld method to the analysis of anhydrous cement," *Cem. Concr. Res.*, vol. 41, no. 2, pp. 133–148, 2011.

[18] Y. P. Stetsko, N. Shanahan, and A. Zayed, "Quantification of supplementary cementitious content in blended Portland cement using an iterative Rietveld – PONKCS technique research papers," pp. 1–10, 2017.

[19] M. F. Brigatti, E. Galan, and B. K. G. Theng, "Structures and Mineralogy of Clay Minerals," in *Developments in Clay Science*, vol. 1, F. Bergaya, B. K. G. Theng, and G. Lagaly, Eds. Elsevier Ltd., 2006, pp. 19–86.

[20] J. Russell and A. Fraser, "Infrared Methods," in *Clay mineralogy: spectroscopic and chemical determinative methods*, M. J. Wilson, Ed. Oxford, UK: Chapman & Hall, 1994, pp. 11–67.

[21] R. Prost, A. Dameme, E. Huard, J. Driard, and J. P. Leydecker, "Infrared study of structural OH in kaolinite, dickite, nacrite, and poorly crystalline kaolinite at 5 to 600 K," *Clays Clay*

Miner., vol. 37, no. 5, pp. 464–468, 1989.

[22] L. V. Prandel, N. M. P. Dias, S. da Costa Saab, A. M. Brinatti, N. F. B. Giarola, and L. F. Pires, "Characterization of kaolinite in the hardsetting clay fraction using atomic force microscopy, X-ray diffraction, and the Rietveld method," *J. Soils Sediments*, vol. 17, no. 8, pp. 2144–2155, 2017.

[23] L. V. Prandel, S. C. Saab, N. F. B. Giarola, and A. M. Brinatti, "Analysis of kaolinite isomorphic substitution and microstrain in hardsetting soils horizons through X-ray diffraction and the Rietveld method," in *Proceedings of the International Symposium on Crystallography*, 2015, pp. 65–65.

[24] F. Bergaya and G. Lagaly, "General introduction: Clays, clay minerals, and clay science," in *Developments in Clay Science*, vol. 1, F. Bergaya, B. K. G. Theng, and G. Lagaly, Eds. Elsevier Ltd., 2006, pp. 1–19.

[25] H. G. Dill, "Kaolin: Soil, rock and ore: From the mineral to the magmatic, sedimentary and metamorphic environments," *Earth-Science Rev.*, vol. 161, pp. 16–129, 2016.

[26] S. Vyazovkin, "Thermogravimetric Analysis," in *Characterization of Materials*, 2012, pp. 177–211.

[27] A. Alujas, R. Fernández, R. Quintana, K. L. Scrivener, and F. Martirena, "Pozzolanic reactivity of low grade kaolinitic clays: Influence of calcination temperature and impact of calcination products on OPC hydration," *Appl. Clay Sci.*, vol. 108, pp. 94–101, May 2015.

[28] B. R. Ilić, A. A. Mitrović, and L. R. Miličić, "Thermal treatment of kaolin clay to obtain metakaolin," *Hem. Ind.*, vol. 64, no. 4, pp. 351–356, 2010.

[29] B. B. Kenne Diffo, A. Elimbi, M. Cyr, J. Dika Manga, and H. Tchakoute Kouamo, "Effect of the rate of calcination of kaolin on the properties of metakaolin-based geopolymers," *J. Asian Ceram. Soc.*, vol. 3, no. 1, pp. 130–138, Mar. 2015.

[30] C. He, B. Osbaeck, and E. Makovicky, "Pozzolanic Reactions of Six Principal Clay Minerals: Activation, Reactivity Assessments and Technological Effects," *Cem. Concr.*

Res., vol. 25, no. 8, pp. 1691–1702, 1995.

[31] A. Shvarzman, K. Kovler, G. S. Grader, and G. E. Shter, "The effect of dehydroxylation/amorphization degree on pozzolanic activity of kaolinite," *Cem. Concr. Res.*, vol. 33, no. 3, pp. 405–416, Mar. 2003.

[32] R. L. Frost and A. M. Vassallo, "The dehydroxylation of the kaolinite clay minerals using infrared emission spectroscopy," *Clays Clay Miner.*, vol. 44, no. 5, pp. 635–651, 1996.

[33] B. Lothenbach, P. T. Durdzinski, and K. De Weerdt, "Thermogravimetric analysis," in *A Practical Guide to Microstructural Analysis of Cementitious Materials*, 2016, pp. 177–211.

[34] J. T. Kloprogge, H. D. Ruan, and R. L. Frost, "Thermal decomposition of bauxite minerals: Infrared emission spectroscopy of gibbsite, boehmite and diaspore," *J. Mater. Sci.*, vol. 37, no. 6, pp. 1121–1129, 2002.

[35] B. L. Karen Scrivener, Ruben Snellings, *A Practical Guide to Microstructural Analysis of Cementitious Materials*. Boca Raton, FL: Taylor & Francis Group LLC, 2016.

[36] F. Avet, R. Snellings, A. Alujas, M. Ben, and K. Scrivener, "Development of a new rapid, relevant and reliable (R3) test method to evaluate the pozzolanic reactivity of calcined kaolinitic clays," *Cem. Concr. Res.*, vol. 85, pp. 1–11, 2016.

[37] P. K. Mehta and P. J. M. Monteiro, *Concrete: Microstructure, Properties and Materials*, 3rd ed. New York, NY: McGraw-Hill, 2006.

[38] A. Teklay, C. Yin, L. Rosendahl, and M. Bøjer, "Calcination of kaolinite clay particles for cement production: A modeling study," *Cem. Concr. Res.*, vol. 61–62, pp. 11–19, 2014.

Chapter 3. Identification of Appropriate Calcination Procedures and Evaluation of Pozzolanic Reactivity

3.1. Introduction

The goal of this research was to identify local sources of clay in the state of Florida that can potentially be used as supplementary cementitious materials (SCMs) in concrete. Clays themselves are not reactive and have to be calcined to obtain a pozzolanic material. It has been reported in the literature that the highest pozzolanic activity results from the calcination of kaolinite. Pozzolanic activity increases with the amount of calcined kaolinite [1]; therefore, the calcination procedure should be such that it results in dehydroxylation of all the kaolinite present in the sample. At the same time, calcination should be done at the lowest temperature possible in order to minimize cost. The objective of this task was to select an appropriate calcination procedure and evaluate pozzolanic activity of the calcined clay samples.

3.2. Selection of Calcination Temperature

On heating, kaolinite transforms from a crystalline compound into amorphous metakaolinite on complete dehydroxylation. This process can be followed by x-ray diffraction (XRD), as well-defined kaolinite peaks decrease in intensity and broaden as it is heated to higher temperatures, and disappear completely as all the kaolinite is converted to metakaolinite. Thermogravimetric analysis (TGA), the results of which are reported in Chapter 2, showed that the end of the dehydroxylation period was observed around 600˚C for all the clay samples, except A1, where a small mass loss was recorded beyond 600˚C. Therefore, A1 was selected for a detailed study of mineral transformations on heating. A1 samples were heated to various temperatures, and the clay fractions (passing the 45-μm sieve) were analyzed with XRD. Clay samples were heated in a 3500-watt Lindberg box furnace capable of heating up to 1100°C. The following temperatures were used in this study: 110, 200, 300, 400, 425, 450, 460, 465, 470, 475, 500, 525, 550, 600, and 800˚C. A step size of 100˚C was selected up to the temperature of 400˚C since TGA analysis showed the onset of dehydroxylation to be at approximately 350˚C, and no other thermal events were recorded at lower temperatures. Between 400˚C and 600˚C, a smaller step size was utilized in order to observe the change in the A1 diffraction pattern during dehydroxylation. After 600˚C, the sample was heated to 800˚C to ensure complete dehydroxylation. XRD scans were

collected using a Phillips X'Pert PW3040 Pro diffractometer equipped with an X'Celerator Scientific detector and a Cu-Kα x-ray source. Tension and current were set to 45 kV and 40 mA, respectively; 5 mm divergence and anti-scatter slits were used in the automatic mode. Scans were collected for the 4-70˚ 2θ angular range, and the samples were rotated at 30 rpm during data collection. The collected diffraction patterns are presented in Figure 3-1. No changes in the diffraction patterns occurred between 110 and 400˚C; therefore, the XRD scans collected at 200˚C and 300˚C were omitted from this figure. The scan at 525˚C was not included either as the changes were minor compared to the data collected at 500˚C and 550˚C. It can be seen from Figure 3-1, that the intensity of kaolinite peaks began to decrease at 460˚C. Peak magnitude continues to decrease with further increase in temperature, and complete disappearance of kaolinite peaks was observed at 600˚C. No significant changes in the XRD pattern was observed with the increase in temperature from 600˚C to 800˚C. Therefore, 600˚C was selected as the calcination temperature for all the clay samples.

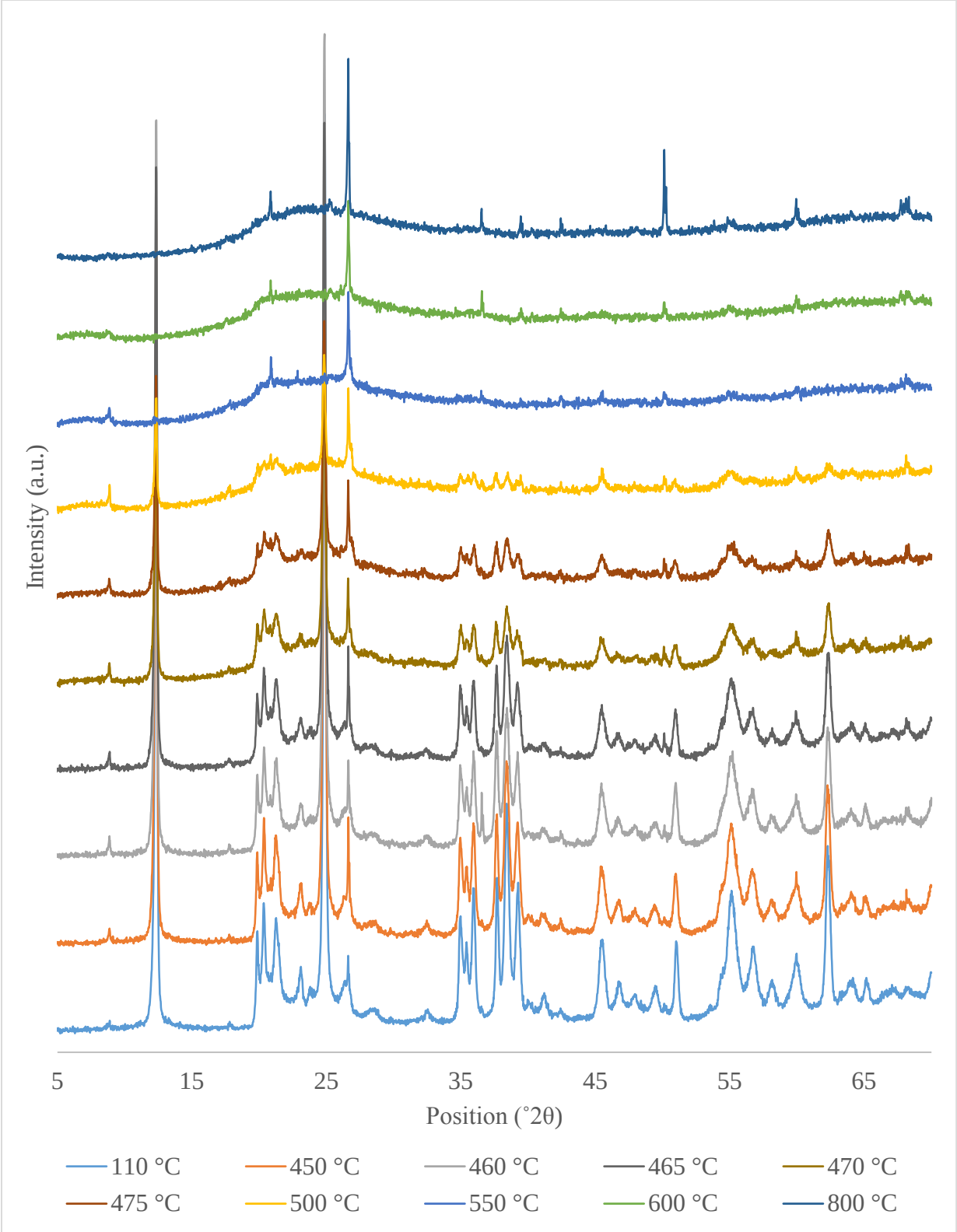

Figure 3-1: XRD patterns of A1 clay heated to different temperatures

3.3. Calcination Procedure

The unsieved material collected from field was used for calcination. The samples were calcined in ceramic crucibles at 600°C for 1 hour in the Lindberg box furnace and allowed to cool to room temperature. The box furnace was equipped with a basic Eurotherm controller without any controlled heating rate capability. The heating rate of this furnace was calculated to be approximately 20°C/min. After calcination, the material was gently ground by hand with mortar and pestle in order to break up the clumps. A portion of the calcined material was sieved on the 45-μm sieve, and the fraction finer than 45 μm was analyzed by XRD to ensure complete calcination for each sample.

In addition to heating at 600˚C, all the samples were also calcined at 800˚C to ensure complete calcination and analyzed with XRD. The XRD scans were collected using the settings described in Section 3.2 and analyzed using Rietveld refinement. The MAC value for the calcined fraction finer than 45 μm was calculated based on chemical oxide analysis reported in Table 2-2, except the loss on ignition (LOI) content was not taken into account as any water would have been lost during the calcination process.

XRD scans were analyzed using Rietveld refinement in order to calculate the amorphous contents of the calcined clays, which are listed in Table 3-1. Since dehydroxylation can only occur in the clay phases, amorphous content was calculated excluding quartz. On dehydroxylation, clay minerals, including kaolinite, become amorphous; therefore, an increase in amorphous content from 600 to 800˚C would indicate a continuing process of dehydroxylation. However, no appreciable differences were observed between samples calcined at these temperatures as can be seen in Table 3-1, which indicates that the dehydroxylation process was completed by 600˚C.

Table 3-1: Amorphous content of the samples calcined at 600°C and 800˚C

Sample ID	Amorphous content (wt%) after calcination at 600˚C	Amorphous content (wt%) after calcination at 800˚C
A1	99.9	99.8
B1	98.0	98.4
B2	96.3	96.8
B3	93.9	94.6
B4	95.7	94.9
C	97.4	97.5
D1	94.8	94.6
E	95.0	94.2
F	95.9	96.0
G	96.5	96.5

3.4. Mortar Compressive Strength

Since the mineralogy of the material calcined at 600°C and 800˚C was very similar, pozzolanic activity was tested only for the 600°C calcination temperature. Pozzolanic activity was evaluated in terms of mortar compressive strength at 10 % cement replacement. A Type I/II portland cement was used in this study. Cement Blaine fineness was determined to be 377 m^2/kg in accordance with ASTM C204 [2]. Cement was also characterized in terms of its oxide chemical composition determined using x-ray fluorescence spectroscopy (XRF) according to ASTM C114 [3], the results of which are listed in Table 3-2. Its potential compound composition was calculated following ASTM C150 [4], and the results are depicted in Table 3-3. The table includes potential phase composition both with and without the adjustment for the limestone addition. Information regarding the percent limestone added to the cement (1.3%) was obtained from the mill certificate.

Table 3-2: Oxide chemical analysis of cement

Analyte	Cement (wt %)
SiO_2	21.19
Al_2O_3	5.00
Fe_2O_3	3.24
CaO	63.26
MgO	0.91
SO_3	3.40
Na_2O	0.12
K_2O	0.23
TiO_2	0.25
P_2O_5	0.22
Mn_2O_3	0.10
SrO	0.08
Cr_2O_3	0.02
ZnO	0.04
L.O.I. (950°C)	1.99
Total	100.07
Na_2O_{eq}	0.27
SO_3/Al_2O_3	0.68

Table 3-3: Bogue-calculated potential compound content of cement

Phase	Without Limestone Correction	With Limestone Correction
C_3S	49	48
C_2S	24	24
C_3A	8	8
C_4AF	10	10
C_4AF+2C_3A	25	25
$C_3S+4.75C_3A$	85	84

Cement mineralogical composition was determined from x-ray diffraction (XRD) measurements conducted in accordance with ASTM C1365 [5]. Prior to XRD measurements, each cement was wet-ground in ethanol in a McCrone micronizing mill to a particle size between 1 and 10 μm. The wet grinding method was used to minimize temperature increases during grinding to avoid dehydration of gypsum to hemihydrate or anhydrite. The samples were then dried in an oven at 40°C.

Selective dissolutions were performed on the as-received cement in order to aid the identification of the minor phases as well as the C_3S and C_3A crystal structures. Salicylic acid/methanol (SAM) extraction was performed to dissolve the silicates and free lime and to isolate a concentrated residue of aluminates, ferrites, and minor phases, such as periclase, carbonates, alkali sulfates, and double alkali sulfates ([6], [7]). Potassium hydroxide/sucrose extraction was used to dissolve aluminates and ferrites and obtain a residue of C_3S, C_2S, alkali sulfates, and MgO [6]. XRD scans were performed using the same settings as described in Section 3.2, except the angular range was 7 - 70° 2θ. Phase quantification was performed using the Rietveld refinement functionality of the PANalytical HighScore Plus 4.5 software. An external standard method was used to calculate the amorphous content of cements ([8]–[11]). Corundum (Standard Reference Material 676a) obtained from the National Institute of Standards and Technology (NIST) was used as an external standard in this study. Mass absorption coefficients (MAC) of corundum and cement were calculated using the MAC calculator functionality in the PANalytical HighScore Plus 4.5 software. The MAC value for cement was based on its chemical oxide compositions listed in Table 3-2. Loss on ignition content was attributed to carbonate decomposition and release of CO_2. The results of cement phase quantification using Rietveld analysis are listed in Table 3-4. The values of C_3S, C_3A and ferrite determined through XRD were lower compared to the Bogue calculation, while the amount of C_2S was higher. The discrepancy between the Bogue calculation and XRD is well-established in the literature ([6], [12], [13]).

Table 3-4: Cement phase composition using XRD

Phase	Cement (wt .%)	σ
C_3S	42.9	0.1
C_2S	30.2	0.1
C_3A	5.8	0.1
Ferrite	9.7	0.1
Gypsum	5.0	0.2
Hemihydrate	1.0	0.1
Calcite	1.2	0.2
Portlandite	0.5	0.1
Amorphous/ unidentified	3.7	

Mortar cubes were prepared following ASTM C109 [14] and ASTM C305 [15], except the water-to-cementitious materials (w/cm) ratio. ASTM C109 [14] specifies that when cementitious materials other than portland cement are used in preparing mortar, the amount of mixing water should be adjusted to maintain a constant flow of 110 ± 5. However, w/cm is a major factor affecting compressive strength [16]. Since the objective of this study was to compare compressive strength development of mortars prepared with different calcined clays, w/cm ratio was maintained constant at 0.485 in order to eliminate it as a variable. After demolding, the cubes were stored in saturated lime solution and their compressive strengths were tested at 7 and 28 days.

Since calcination was done on the unsieved material, calcined samples contained both the clay and the sand fractions as determined in Section 2.3.1. In order to maintain the amount of cement replacement by the calcined clay constant, the total amount of calcined material was calculated using the values for clay fraction listed in Table 2-1. The amount of Ottawa sand was then adjusted to account for the amount of sand contained in the calcined material. The mix designs for all the mortars are listed in Table 3-5. The following naming convention was used for the mix designs: 10X-600-1, where 10 was the cement replacement level (percent by weight), X was the name of the calcined material, 600 was the calcination temperature (°F) and 1 referred to the duration of calcination (hours).

The mix designs used for a selected set of control mixtures are listed in Table 3-6. The common Control mortar contained only portland cement and Ottawa sand. Individual control mixtures were prepared for the first five calcined clays that contained only portland cement, but the same portion of Ottawa sand was replaced by the sand from the calcined material as in the respective calcined clay mixture (Table 3-5). The individual controls were only tested at 7 days.

Table 3-5: Mix design proportions for calcined clay mortars

	A1	B1	B2	B3	B4	C	D1	E	F	G
Cement (g)	450	450	450	450	450	450	450	450	450	450
Ottawa sand (g)	1,207	1,271	1,159	1,224	1,236	1,176	1,282	947	1,213	1,223
Calcined material (g)	217	153	266	200	188	248	142	477	211	201
Clay from calcined material (g)	50	50	50	50	50	50	50	50	50	50
Sand from calcined material (g)	167	103	216	150	138	198	92	427	161	151
Water (g)	242	242	242	242	242	242	242	242	242	242

Table 3-6: Mix design proportions for calcined clay control mortars

	Control	Control A1	Control B1	Control B2	Control B3	Control B4
Cement (g)	500	500	500	500	500	500
Ottawa sand (g)	1,374	1,207	1,271	1,159	1,224	1,236
Sand from calcined material (g)	0	167	103	216	150	138
Water (g)	242	242	242	242	242	242

Figure 3-2 presents the compressive strength results for all the calcined clay mixtures and the Control. Additionally, the percentages of the common Control mortar were calculated for all the clay mixtures, and the results are listed in Table 3-7. It can be seen that at 7 days, compressive strengths of the calcined clay mortars were greater than 75% for all the samples, except 10B3-600-1. However, by 28 days, the strength activity index was above 76% for all the mixtures. Clay mixtures were also compared to a mortar mixture containing 10% Class F fly ash (10FA), the results for which were reported in an earlier study [17] and were, respectively, 84% and 86% of the fly ash control at 7 and 28 days. A majority of the clay mortars showed similar performance to that of 10FA at 7 days, with exception of 10B1-600-1 and 10B3-600-1 mixtures. At 28 days, half of the clay mortars were comparable to the fly ash mix, with 10B1-600-1, 10B3-600-1, 10B4-600-1 and 10C-600-1 showing lower values. However, this difference could be due to the replacement of Ottawa sand.

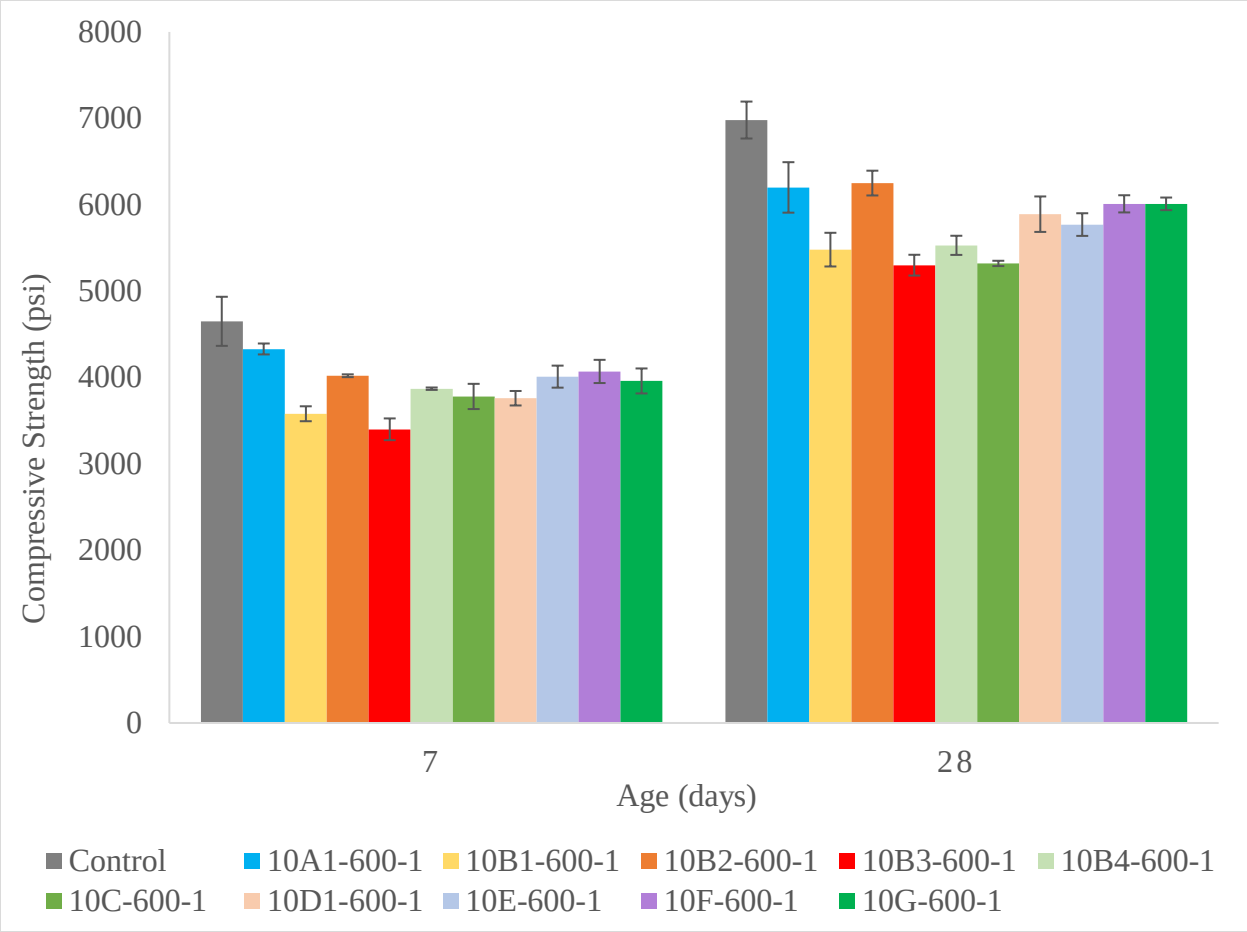

Figure 3-2: Compressive strength of mortar cubes prepared with 10% calcined clay cement replacement

Table 3-7: Strength activity index based on the common control mixture

Mix ID	Strength Activity Index	
	7 days	28 days
10A1-600-1	93 %	89 %
10B1-600-1	77 %	79 %
10B2-600-1	86 %	90 %
10B3-600-1	73 %	76 %
10B4-600-1	83 %	79 %
10C-600-1	81 %	76 %
10D1-600-1	81 %	84 %
10E-600-1	86 %	83 %
10F-600-1	88 %	86 %

In order to eliminate the variability in the sand gradation, compressive strengths of the first five calcined clay mixtures were compared to their respective controls, where a portion of Ottawa sand was replaced with the sand coming from the calcined material (Figure 3-3). When compressive strengths of the calcined clay mixtures were compared to their respective controls, the strength activity indices at 7 days were higher than 75%, even for the 10B3-600-1 mixture, (Table 3-8). Compressive strengths of Control, A1, B2, and B4 were very similar to that of the common Control mixture, while the compressive strengths of Control, B1, and B3 were lower, which is consistent with the trend observed in Figure 3-2 at 7 days, where 10B1-600-1 and 10B3-600-1 mixtures had the lowest compressive strengths. Nevertheless, performance of all the mixes was very similar to that of 10FA.

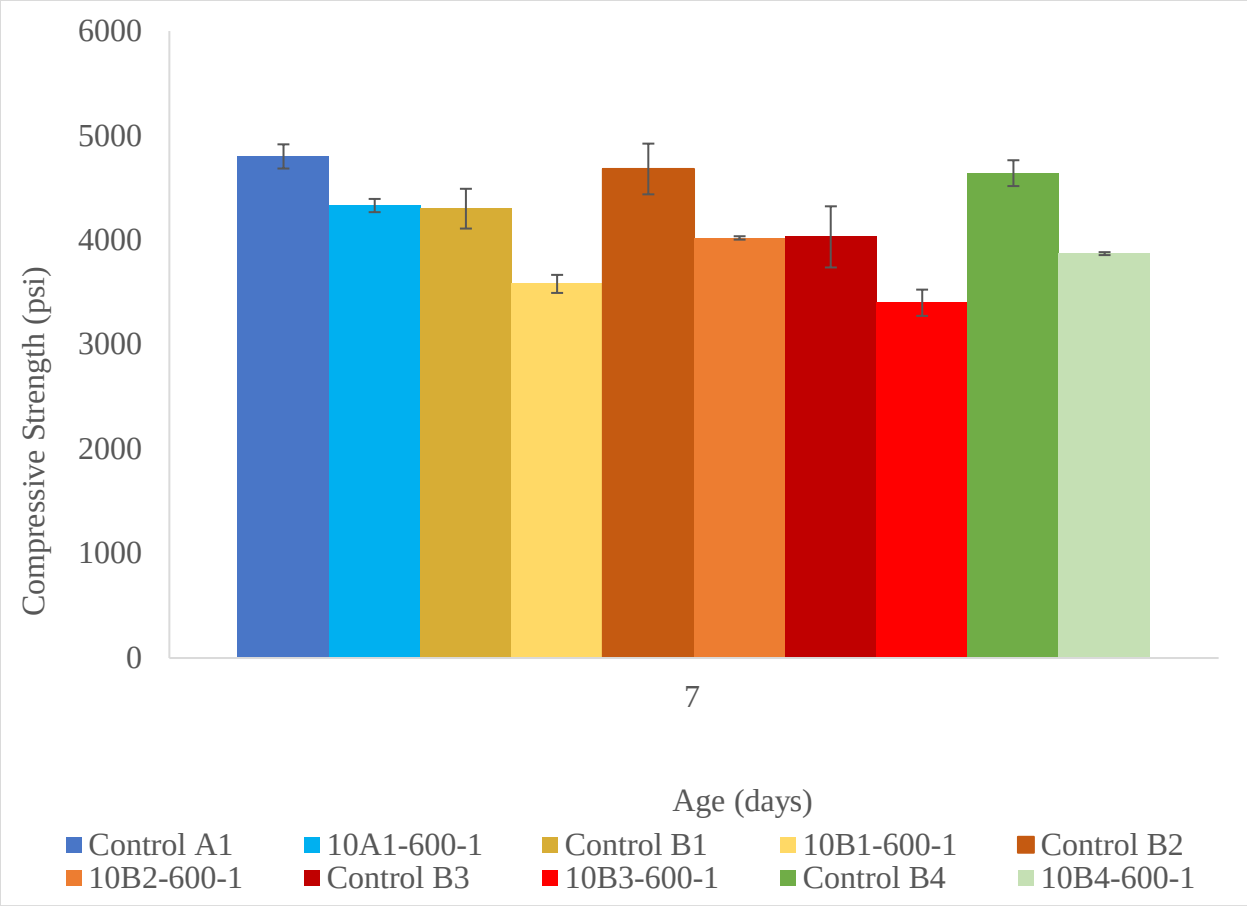

Figure 3-3: Comparison of 7-day compressive strength

Table 3-8: Strength activity index based on the individual controls

Mix ID	Strength Activity Index at 7 days
10A1-600-1	90 %
10B1-600-1	83 %
10B2-600-1	86 %
10B3-600-1	84 %
10B4-600-1	83 %

3.5. Conclusions

A detailed step-wise temperature study performed for A1 clay showed that complete dehydroxylation occurs at 600˚C. All the clays were calcined at 600 and 800˚C and their amorphous content was quantified using Rietveld refinement. No change in amorphous content was detected on heating above 600˚C, confirming that all the clays were completely dehydroxylated at this temperature.

Pozzolanic activity of the material calcined at 600˚C was evaluated by compressive strength testing at 7 and 28 days. The results showed that the Florida kaolinitic clays obtained are capable of being calcined to produce a pozzolanic material that can be used to replace portland cement in concrete and yield similar compressive strengths to those achieved with 10% Class F fly ash, and therefore, appear to be suitable for producing a supplementary cementitious material for use in concrete.

3.6. References

[1] N. Amin, S. Alam, and S. Gul, "Assessment of pozzolanic activity of thermally activated clay and its impact on strength development in cement mortar," *RSC Adv.*, vol. 5, no. 8, pp. 6079–6084, Dec. 2015.

[2] ASTM C204-16, *Standard Test Method for Fineness of Hydraulic Cement by Air Permeability Apparatus*. West Conshohocken, Pa., Pa.: ASTM International, 2016.

[3] ASTM C114-13, *Standard Test Method for Chemical Analysis of Hydraulic Cement*, West Conshohocken, PA: ASTM International, 2013.

[4] ASTM C150/C150M-16, *Standard Specification for Portland Cement*. West Conshohocken, Pa.: ASTM International, 2016.

[5] ASTM C1365-06 (2011), *Standard Test Method for Determination of the Proportion of Phases in Portland Cement and Portland-Cement Clinker Using X-Ray Powder Diffraction Analysis*, West Conshohocken, PA: ASTM International, 2016.

[6] P. E. Stutzman, *Guide for X-Ray Powder Diffraction Analysis of Portland Cement and*

Clinker, Gaithersburg, MD, 1996.

[7] W. A. Gutteridge, "On the Dissolution of the Interstitial Phases in Portland Cement," *Cem. Concr. Res.*, vol. 9, no. 3, pp. 319–324, 1979.

[8] B. H. O'Connor and M. D. Raven, "Application of the Rietveld Refinement Procedure in Assaying Powdered Mixtures," *Powder Diffr.*, vol. 3, no. 1, pp. 2–6, Jan. 1988.

[9] D. Jansen, C. Stabler, F. Goetz-Neunhoeffer, S. Dittrich, and J. Neubauer, "Does Ordinary Portland Cement Contain Amorphous Phase? A Quantitative Study Using an External Standard Method," *Powder Diffr.*, vol. 26, no. 1, pp. 31–38, Mar. 2011.

[10] M. A. G. Aranda, A. G. De la Torre, and L. Leon-Reina, "Rietveld Quantitative Phase Analysis of OPC Clinkers, Cements and Hydration Products," *Reviews in Mineralogy and Geochemistry*, vol. 74, no. 1. pp. 169–209, 2012.

[11] I. C. Madsen, N. V. Y. Scarlett, and A. Kern, "Description and survey of methodologies for the determination of amorphous content via X-ray powder diffraction," *Zeitschrift für Krist.*, vol. 226, no. 12, pp. 944–955, Dec. 2011.

[12] P. Stutzman, "Powder diffraction analysis of hydraulic cements: ASTM Rietveld round-robin results on precision," *Powder Diffr.*, vol. 20, no. 2, pp. 97–100, Jun. 2005.

[13] H. F. W. Taylor, *Cement Chemistry*, 2nd ed. London, UK: Thomas Telford Publishing, 1997.

[14] ASTM C109/ C109M-16a, *Standard Test Method for Compressive Strength of Hydraulic Cement Mortars (Using 2-in. or [50-mm] Cube Specimens)*, West Conshohocken, PA: ASTM International, 2016.

[15] ASTM C305-14, *Standard Practice for Mechanical Mixing of Hydraulic Cement Pastes and Mortars of Plastic Consistency*, West Conshohocken, PA: ASTM International, 2014.

[16] S. Mindess, J. F. Young, and D. Darwin, *Concrete*, 2nd ed. Upper Saddle River, NJ: Prentice Hall, 2003.

[17] A. Zayed, N. Shanahan, V. Tran, A. Markandeya, A. Williams, and A. Elnihum, *Effect of Chemical and Mineral Admixtures on Performance of Florida Structural Concrete*, University of South Florida, Tampa, FL, Florida Department of Transportation, 2016.

Chapter 4. Conclusions and Recommendations

The findings of this study are summarized as follows:

- Field samples were obtained from 20 potential clay sources, a number of which had similar mineralogy based on visual examination of the x-ray diffraction patterns of the material finer than 45 μm. Eleven samples representative of the variation in mineralogy in the collected 20 samples showed that the percentage greater than 45 μm varied from 65 to 80%, indicating that these materials must be beneficially processed before they can comply with the ASTM C618 requirement of a maximum of 34% retained on the 45-μm (325-mesh) sieve. The fractions finer than 45 μm met the ASTM C618 chemical oxide composition requirements: minimum of 70.0% for SiO_2+Al_2O_3+Fe_2O_3 and SO_3 content of less than 4%. The kaolin content of the minus 325-mesh material ranged from approximately 70 to 95%, indicating a good potential of producing a high-quality pozzolanic material on calcination.
- A step-wise temperature study of one of the clays showed that complete dehydroxylation occurs at 600˚C. Amorphous content for all clays after calcination at 600 and 800˚C was quantified using Rietveld refinement. No change in amorphous content was detected on heating above 600˚C, confirming that all the clays were completely dehydroxylated at this temperature.
- Performance of the material calcined at 600˚C was evaluated by compressive strength testing at 7 and 28 days. The results showed that the Florida kaolinitic clays obtained are capable of being calcined to produce a pozzolanic material that can be used to replace portland cement in concrete and yield similar compressive strengths to those achieved with the same amount of Class F fly ash, and therefore, appear to be suitable for producing a supplementary cementitious material for use in concrete.

Based on the findings of this study, it is recommended that Florida Department of Transportation proceed to Phase II of this research in order to further evaluate the effects of calcined clays on the properties of cementitious mixtures, including strength and durability.

Appendix A. Thermogravimetric Analysis and Differential Thermogravimetry Curves for Clay Samples

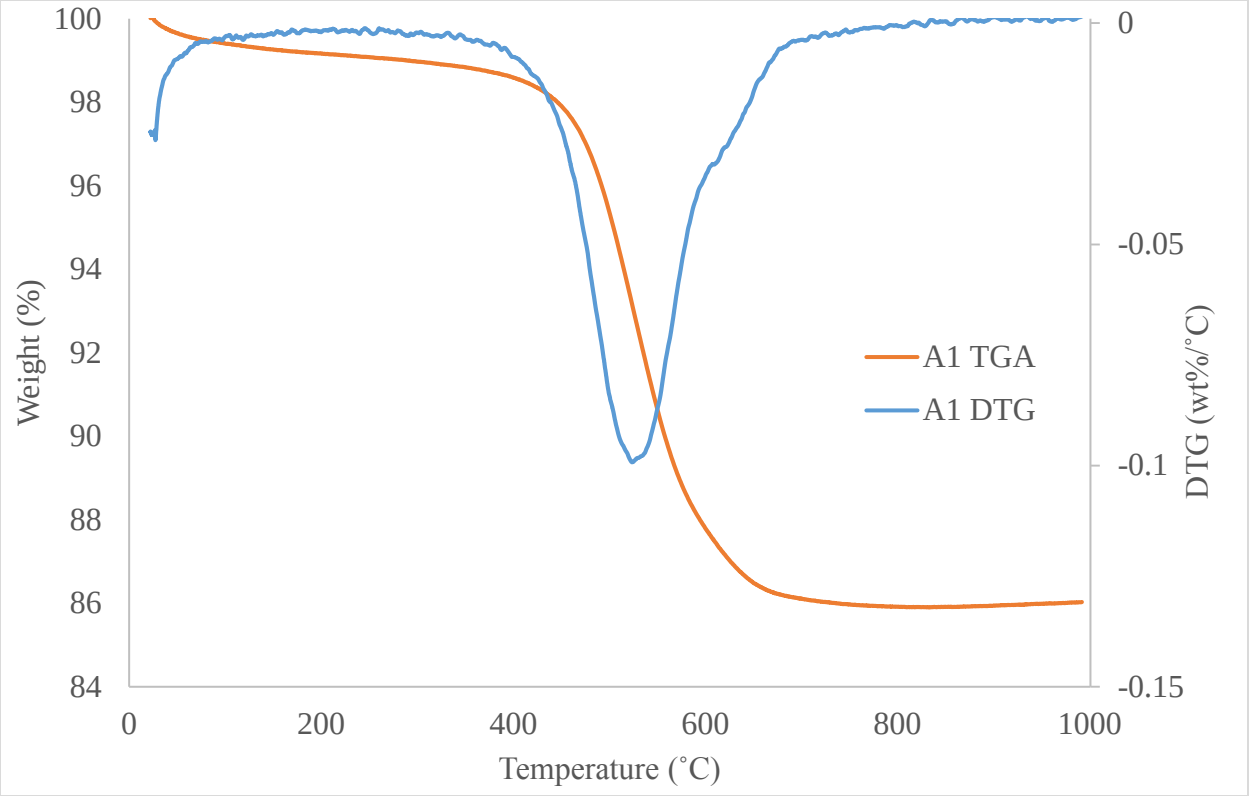

Figure A-1: TGA and DTG curves for A1 clay sample

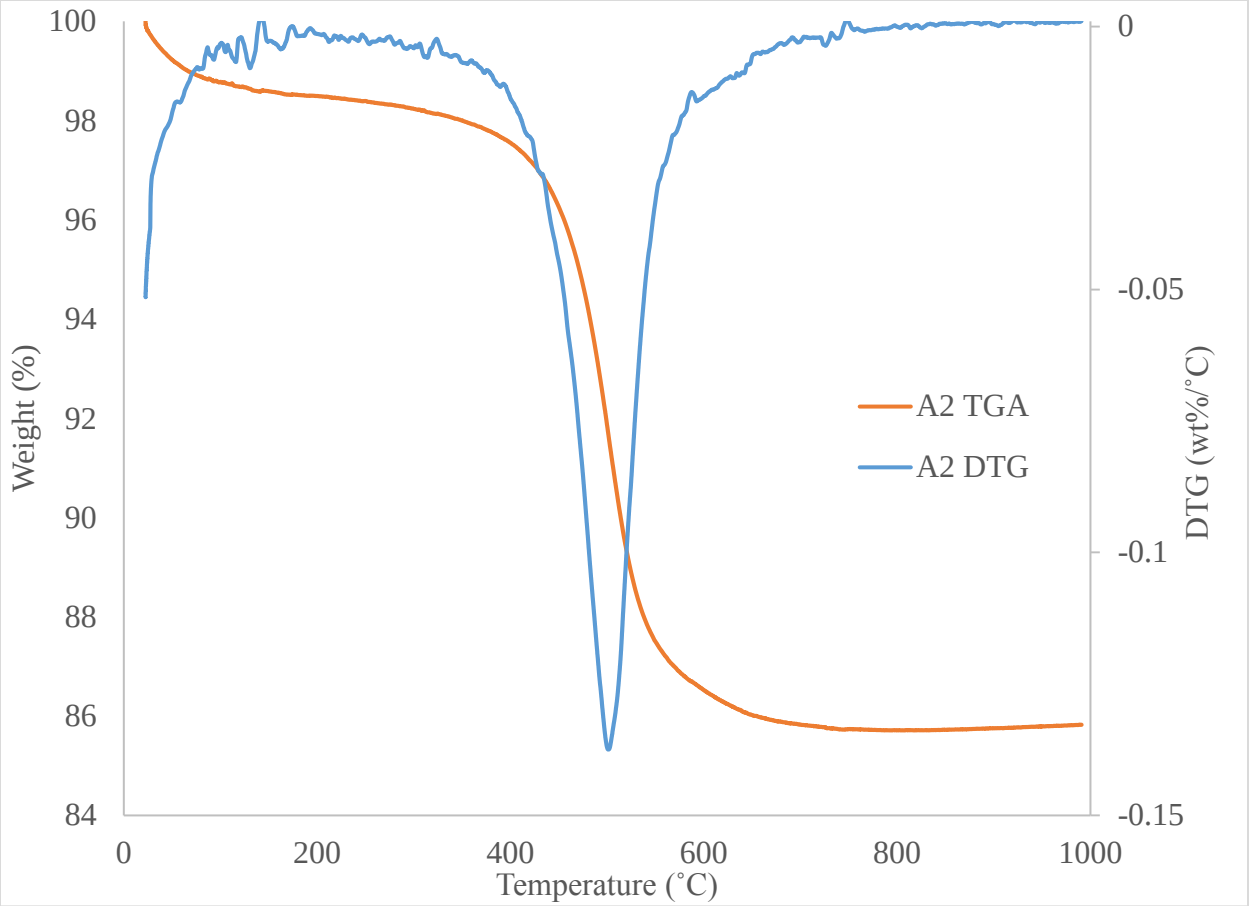

Figure A-2: TGA and DTG curves for A2 clay sample

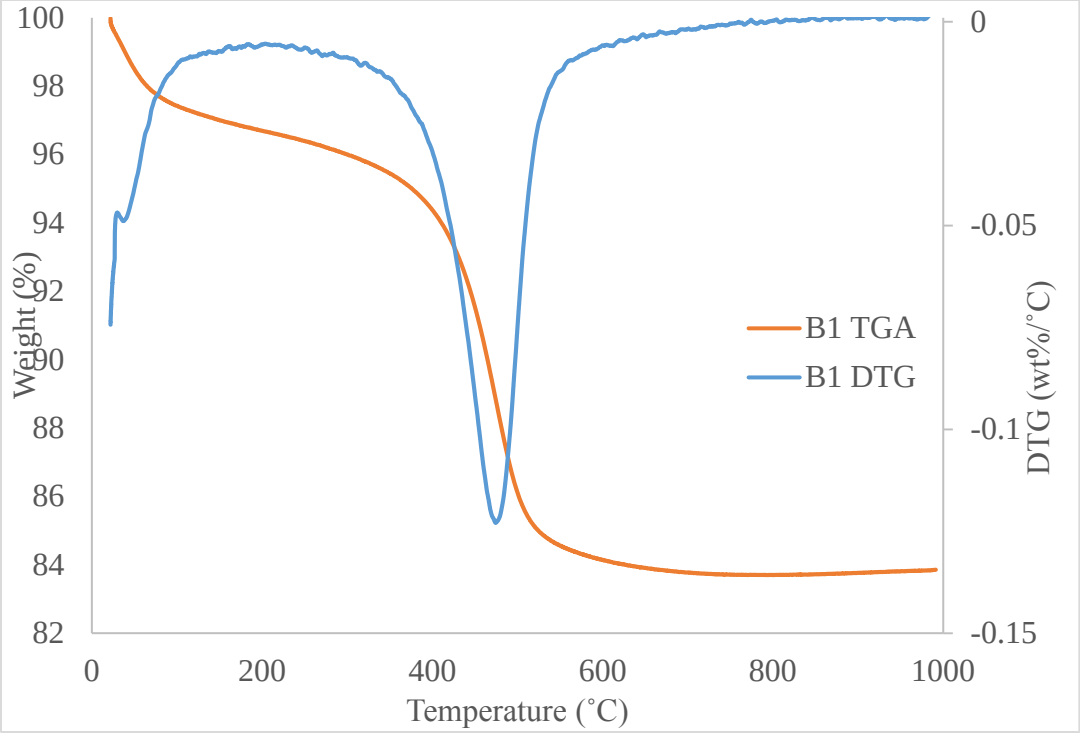

Figure A-3: TGA and DTG curves for B1 clay sample

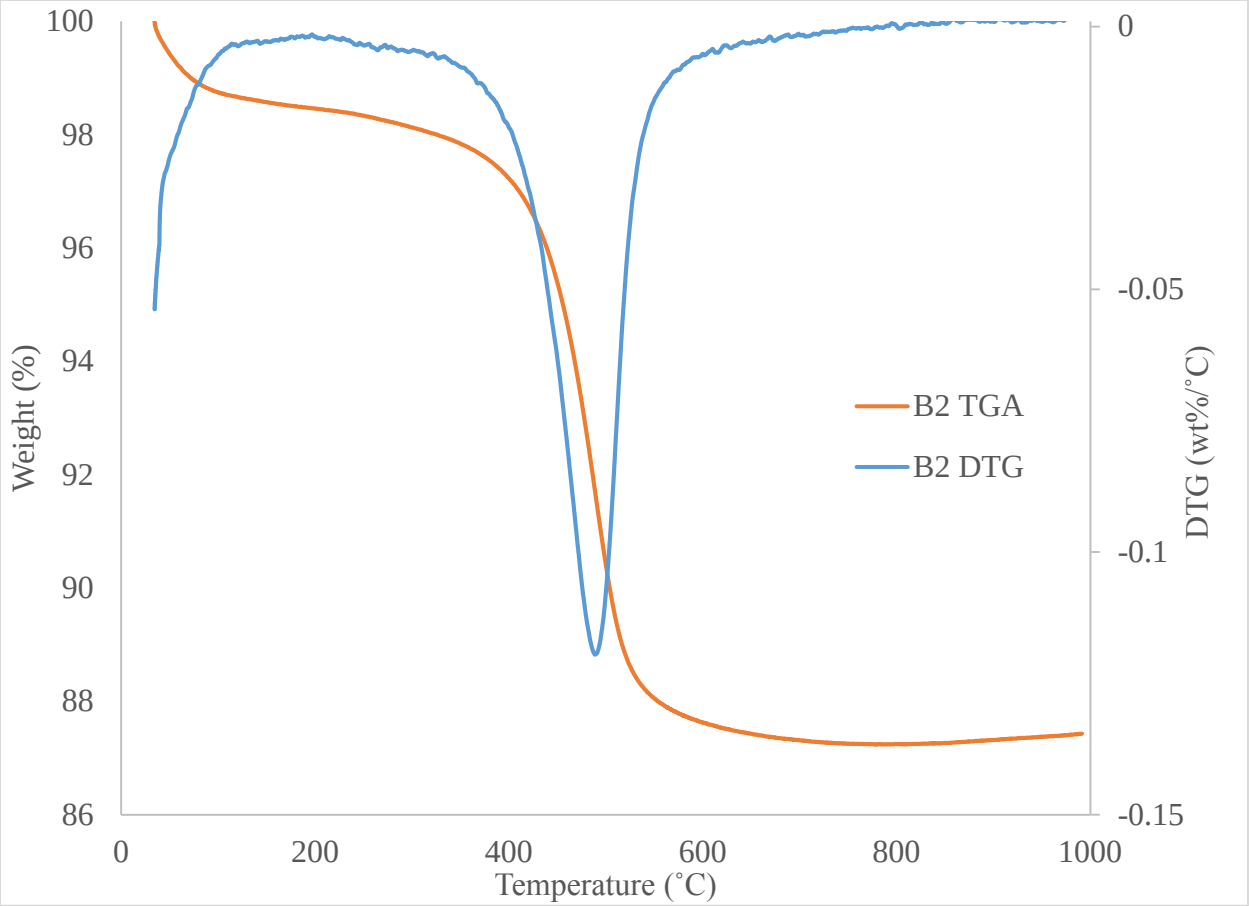

Figure A-4: TGA and DTG curves for B2 clay sample

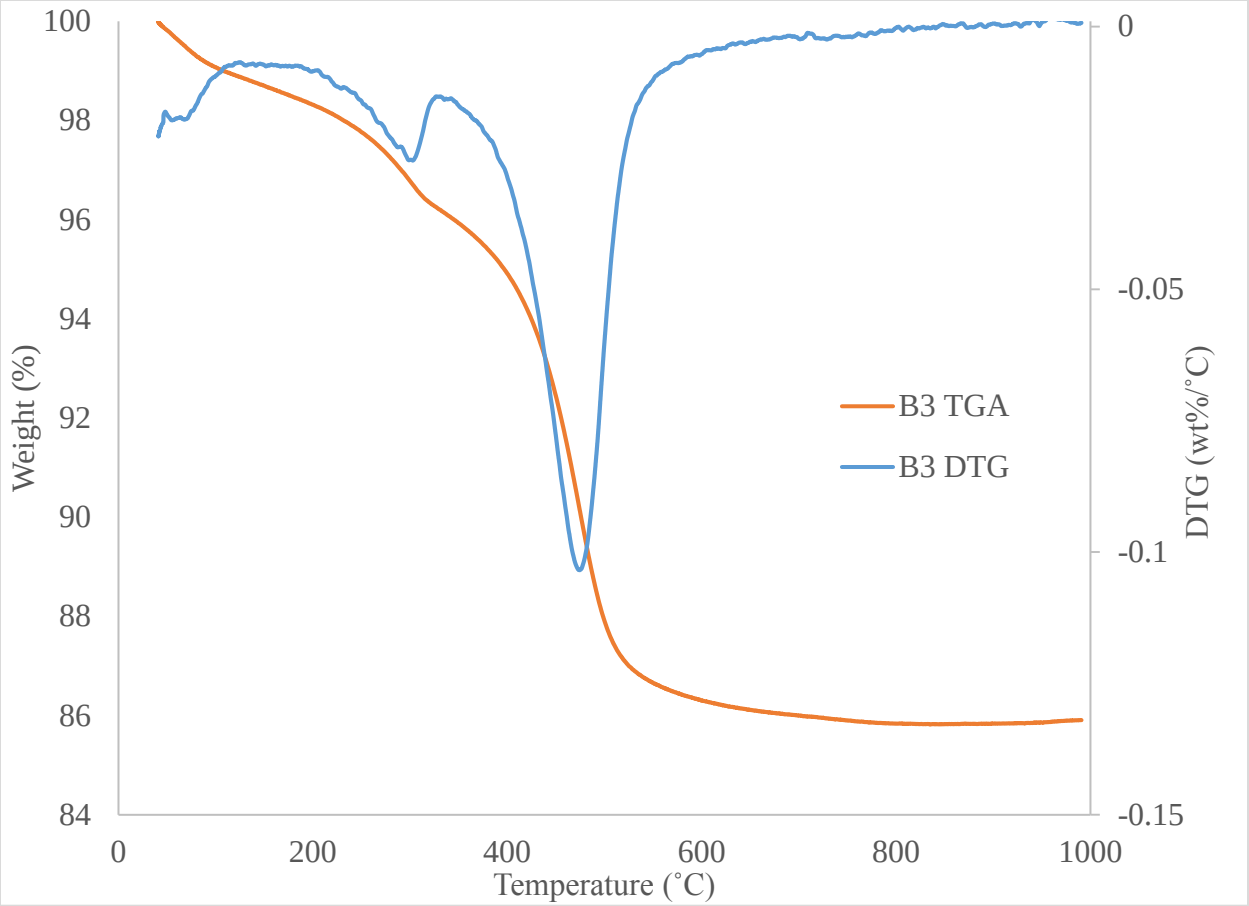

Figure A-5: TGA and DTG curves for B3 clay sample

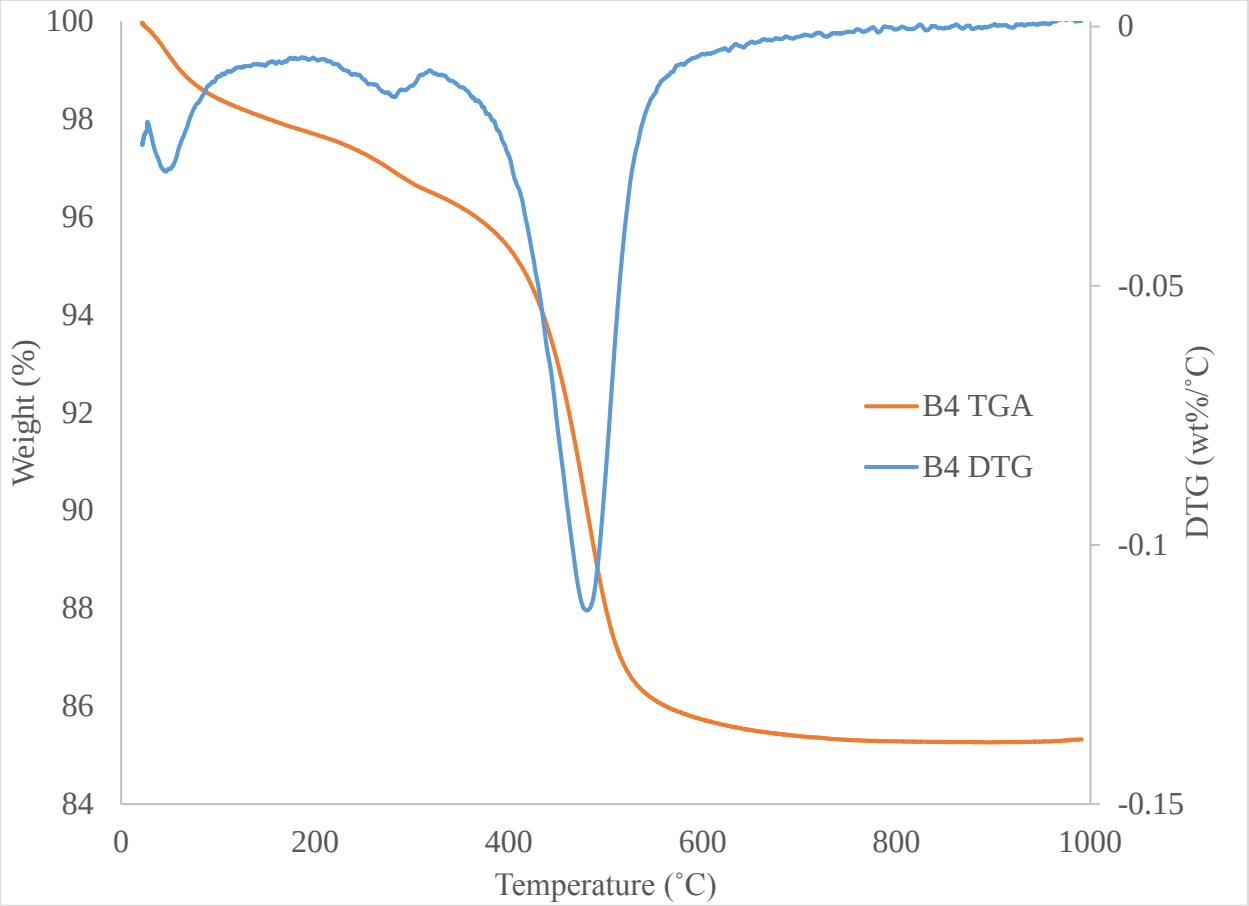

Figure A-6: TGA and DTG curves for B4 clay sample

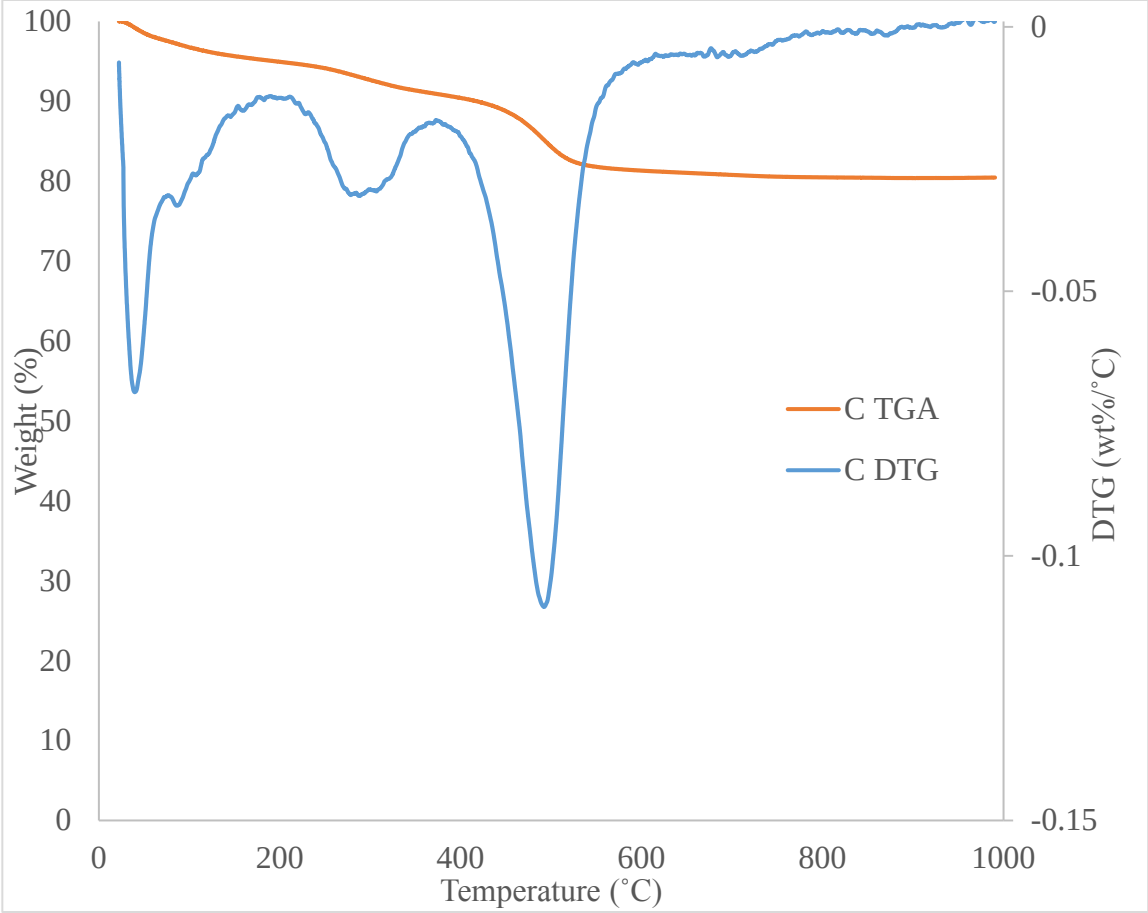

Figure A-7: TGA and DTG curves for C clay sample

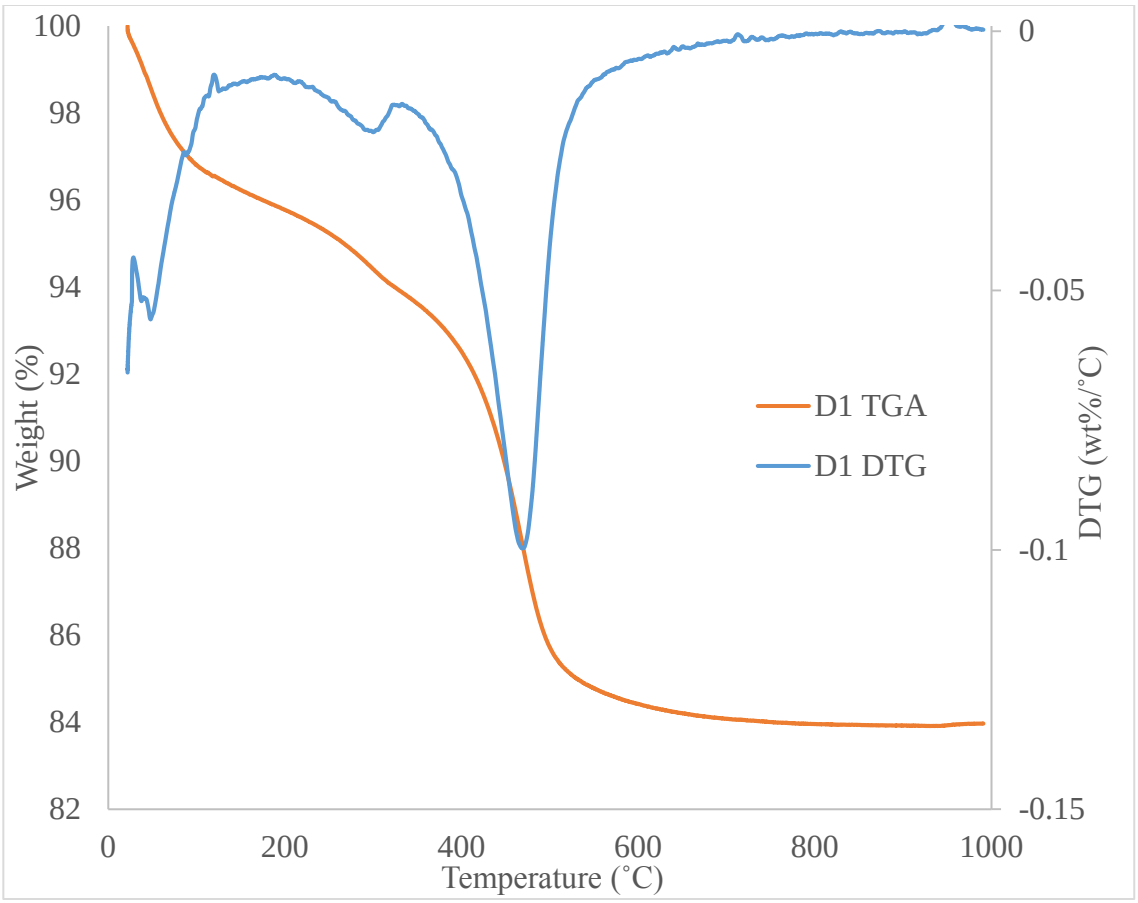

Figure A-8: TGA and DTG curves for D1 clay sample

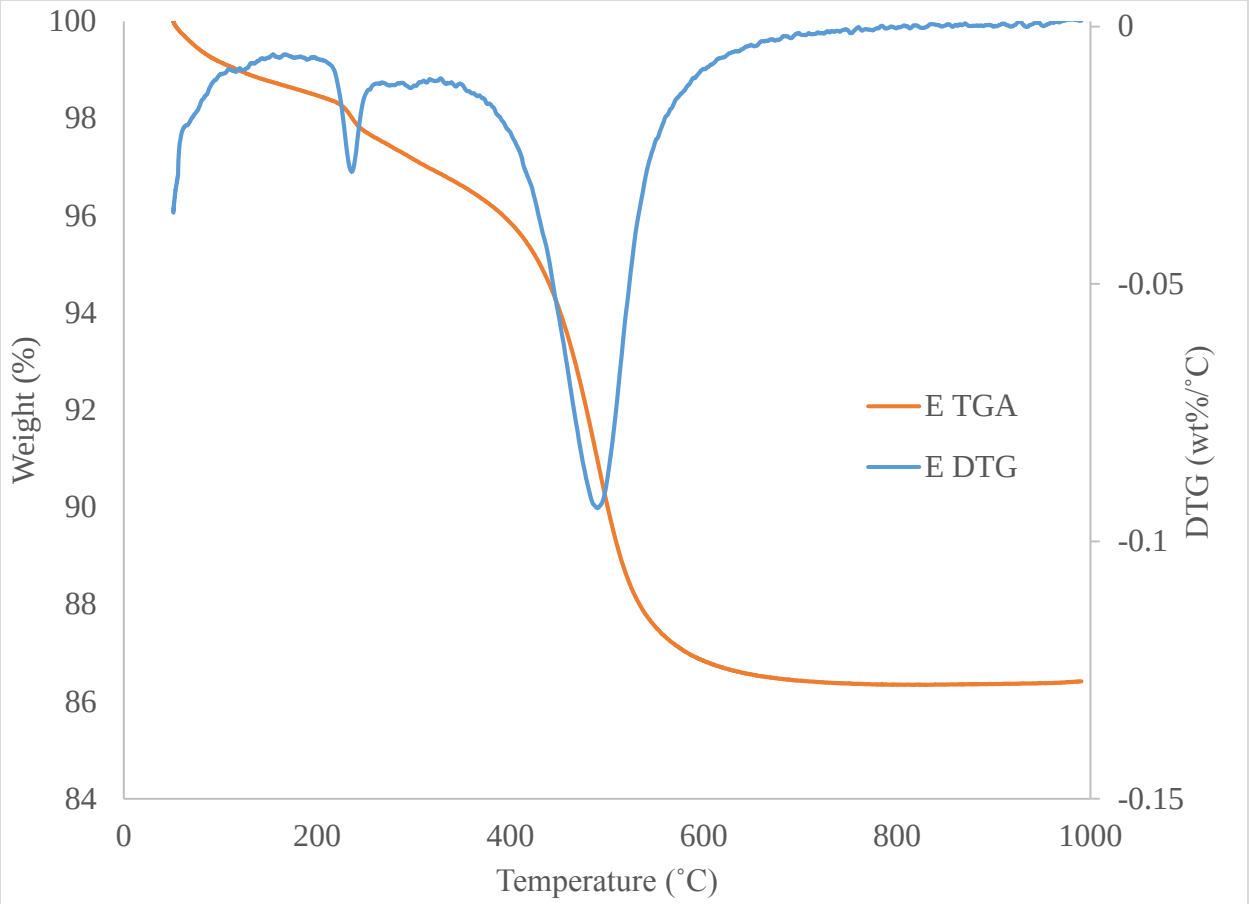

Figure A-9: TGA and DTG curves for E clay sample

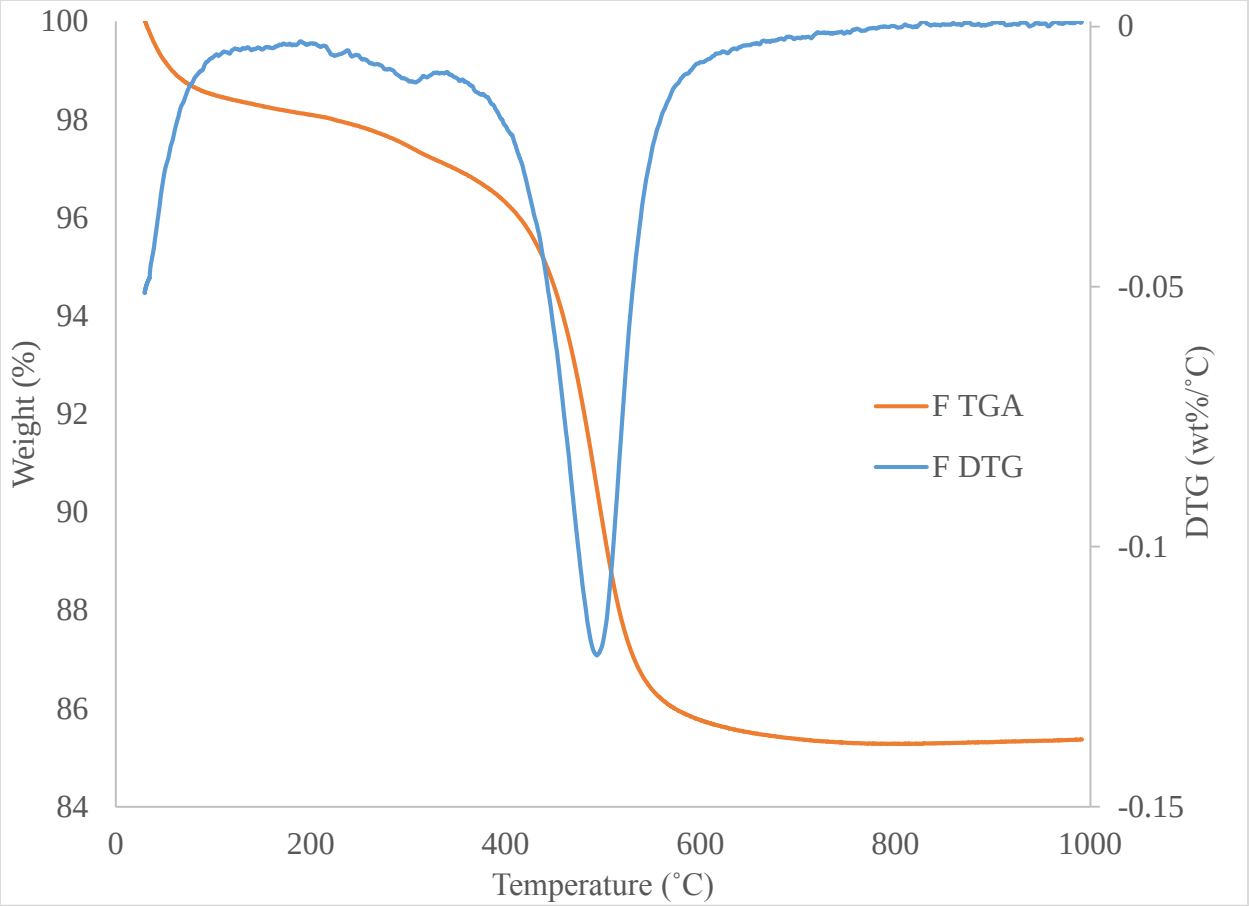

Figure A-10: TGA and DTG curves for F clay sample

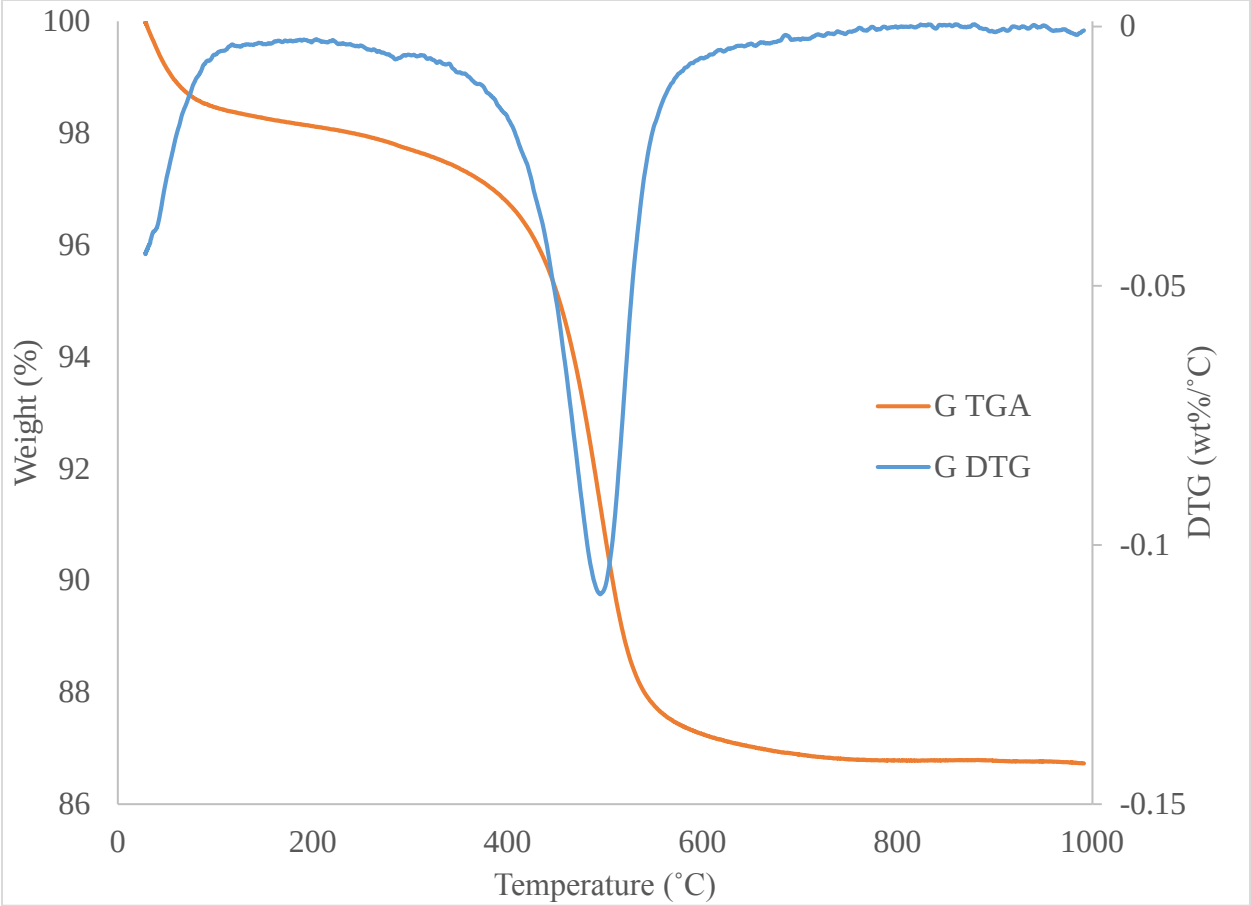

Figure A-11: TGA and DTG curves for G clay sample